



Contents lists available at ScienceDirect

European Journal of Medicinal Chemistry

journal homepage: www.elsevier.com/locate/ejmech

Research paper



Synthesis, computational and experimental pharmacological studies for (thio)ether-triazine 5-HT₆R ligands with noticeable action on AChE/BChE and chalcogen-dependent intrinsic activity in search for new class of drugs against Alzheimer's disease

Kinga Czarnota-Łydka^{a,b}, Sylwia Sudol-Talaj^{a,b}, Katarzyna Kucwaj-Brysz^a, Rafał Kurczab^c, Grzegorz Satała^c, Modesto de Candia^d, Francesco Samarelli^d, Cosimo Damiano Altomare^d, Alessia Carocci^d, Alexia Barbarossa^d, Ewa Żesławska^e, Monika Gluch-Lutwin^f, Barbara Mordyl^f, Monika Kubacka^g, Natalia Wilczyńska-Zawal^h, Magdalena Jastrzębska-Więsek^h, Anna Partyka^h, Nadia Khan^{a,b,j}, Małgorzata Więcek^a, Wojciech Nitekⁱ, Ewelina Honkisz-Orzechowska^a, Gniewomir Latacz^a, Anna Wesolowska^h, Antonio Carrieri^{*d}, Jadwiga Handzlik^{a,*}

^a Department of Technology and Biotechnology of Drugs, Jagiellonian University, Medical College, Medyczna 9, PL 30-688, Krakow, Poland

^b Doctoral School of Medical and Health Sciences, Jagiellonian University Medical College, św. Łazarza 15, 31-530, Krakow, Poland

^c Maj Institute of Pharmacology Polish Academy of Sciences, Department of Medicinal Chemistry, Smętna 12, PL 31-343, Krakow, Poland

^d Department of Pharmacy-Drug Sciences, University of Bari Aldo Moro, via E. Orabona 4, 70125, Bari, Italy

^e Pedagogical University of Krakow, Institute of Biology and Earth Sciences, Podchorążych 2, PL 30-084, Krakow, Poland

^f Department of Pharmacobiology, Jagiellonian University, Medical College, Medyczna 9, PL 30-688, Krakow, Poland

^g Department of Pharmacodynamics, Jagiellonian University, Medical College, Medyczna 9, PL 30-688, Krakow, Poland

^h Department of Clinical Pharmacy, Jagiellonian University, Medical College, Medyczna 9, PL 30-688, Cracow, Poland

ⁱ Faculty of Chemistry, Jagiellonian University, Gronostajowa 2, PL 30-387, Krakow, Poland

^j Department of Pathophysiology, Jagiellonian University, Medical College, Czysza 18, PL 30-688, Krakow, Poland

ARTICLE INFO

Keywords:

5-HT₆ serotonin receptors
1,3,5-Triazine
Thioether
ADME-Tox
Behavioral tests

ABSTRACT

Alzheimer's disease is becoming a growing problem increasing at a tremendous rate. Serotonin 5-HT₆ receptors appear to be a particularly attractive target from a therapeutic perspective, due to their involvement not only in cognitive processes, but also in depression and psychosis. In this work, we present the synthesis and broad biological characterization of a new series of 18 compounds with a unique 1,3,5-triazine backbone, as potent 5-HT₆ receptor ligands. The main aim of this research is to compare the biological activity of the newly synthesized sulfur derivatives with their oxygen analogues and their *N*-demethylated *O*- and *S*-metabolites obtained for the first time. Most of the new triazines displayed high affinity ($K_i < 200$ nM) and selectivity towards 5-HT₆R, with respect to 5-HT_{2A}R, 5-HT₇R, and D₂R, in the radioligand binding assays. For selected, active compounds crystallographic studies, functional bioassays, and ADME-Tox profile *in vitro* were performed. The exciting novelty is that the sulfur derivatives exhibit an agonistic mode of action contrary to all other compounds obtained to date in this chemical class herein and previously reported. Advanced computational studies indicated that this intriguing functional shift might be caused by presence of chalcogen bonds formed only by the sulfur atom. In addition, the

* Corresponding authors.

E-mail addresses: kinga.czarnota@doctoral.uj.edu.pl (K. Czarnota-Łydka), s.sudol@doctoral.uj.edu.pl (S. Sudol-Talaj), katarzyna.kucwaj@uj.edu.pl (K. Kucwaj-Brysz), kurczab@if-pan.krakow.pl (R. Kurczab), satala@if-pan.krakow.pl (G. Satała), modesto.decandia@uniba.it (M. de Candia), francesco.samarelli@uniba.it (F. Samarelli), cosimodamiano.altomare@uniba.it (C.D. Altomare), alessia.carocci@uniba.it (A. Carocci), alexia.barbarossa@uniba.it (A. Barbarossa), ewa.zeslawska@up.krakow.pl (E. Żesławska), monika.gluch-lutwin@uj.edu.pl (M. Gluch-Lutwin), barbara.mordyl@uj.edu.pl (B. Mordyl), monika.kubacka@uj.edu.pl (M. Kubacka), natalia.wilczynska@uj.edu.pl (N. Wilczyńska-Zawal), m.jastrzebska-wiesek@uj.edu.pl (M. Jastrzębska-Więsek), annairena.partyka@uj.edu.pl (A. Partyka), nadia.khan@doctoral.uj.edu.pl (N. Khan), malgorzata.wiecek@uj.edu.pl (M. Więcek), wojciech.nitek@uj.edu.pl (W. Nitek), ewelina.honkisz@uj.edu.pl (E. Honkisz-Orzechowska), gniewomir.latacz@uj.edu.pl (G. Latacz), a.wesolowska@uj.edu.pl (A. Wesolowska), antonio.carrieri@uniba.it (A. Carrieri), j.handzlik@uj.edu.pl (J. Handzlik).

<https://doi.org/10.1016/j.ejmech.2023.115695>

Received 17 June 2023; Received in revised form 27 July 2023; Accepted 28 July 2023

Available online 30 July 2023

0223-5234/© 2023 The Authors. Published by Elsevier Masson SAS. This is an open access article under the CC BY-NC-ND license (<http://creativecommons.org/licenses/by-nc-nd/4.0/>).

N-demethylated derivatives have emerged highly potent antioxidants and, moreover, show a significant improvement in metabolic stability compared to the parent structures. The cholinesterase study present micromolar inhibitory AChE and BChE activity for both 5-HT₆ agonist 19 and potent antagonist 5. Finally, the behavioral experiments of compound 19 demonstrated its antidepressant-like properties and slight ability to improve cognitive deficits, without inducing memory impairments by itself. Described pharmacological properties of both compounds (5 and 19) allow to give a design clue for the development of multitarget compounds with 5-HT₆ (both agonist and antagonist)/AChE and/or BChE mechanism in the group of 1,3,5-triazine derivatives.

1. Introduction

Neurodegenerative diseases such as Parkinson's disease, Alzheimer's disease (AD) and other types of dementia constitute one of the most numerous groups of brain disorders due to their incurability [1]. Approximately, 50 million people worldwide struggle with the symptoms of dementia such as memory loss, difficulty concentrating, problems with orientation, emotional disturbances and other cognitive impairments [2]. The most common cause of dementia known to date is AD, which involves the progressive damage and atrophy of neurons [3]. The etiology of AD is still not completely understood and therefore searching for innovative and effective treatment is a great challenge for researchers [4].

The main cause of cognitive decline in AD patients is deterioration of cholinergic neurons in the brain and loss of neurotransmission due to decreased acetylcholine (ACh) synthesis. Therefore, one potential therapeutic strategy is to increase brain acetylcholine levels by inhibiting the biological activity of acetylcholinesterase (AChE) [5]. Hence, 3 out of 4 cognitive enhancing synthetic drugs, currently available to treat Alzheimer's disease are acetylcholinesterase inhibitors (AChE-I). The last one, memantine, is a N-methyl-D47 aspartate (NMDA) receptor antagonist (Fig. 1) [6,7]. Recently, clinical studies have also demonstrated the efficacy of a new immunological approach (the use of monoclonal antibodies that reduce amyloid beta in the brain), which led to the registration of aducanumab (2021 – approved only in the US) and lecanemab (2023) admission on the pharmaceutical market [8]. However, all the above-mentioned therapies are still insufficient as the existing synthetic drugs often have only a short duration of action, moreover, in many cases they do not result in a significant improvement in the quality of

life. On the other hand, the newest biological drugs are very expensive and their efficacy brought a lot of controversy [9].

In recent years, increased attention has been paid to serotonin receptors, in particular those discovered, cloned and characterized at the latest, the 5-HT₆ serotonin receptors (5-HT₆R). These receptors, occurring exclusively in the central nervous system (CNS), have been shown to regulate central cholinergic transmission by modulating primarily GABA and glutamate levels [10], thereby facilitating the secondary release of other neurotransmitters such as dopamine, norepinephrine and acetylcholine. In this context, modulation of the serotonergic system through various signal transduction pathways may be a promising symptomatic strategy for AD [11]. Many preclinical studies indicate that antagonism or even paradoxically agonism of 5-HT₆R can improve cognitive function and restore memory deficits [12].

Despite the vastness of compounds already synthesized and such positive results in the preclinical studies, none of the potential selective 5-HT₆R ligands obtained to date have shown sufficiently high efficacy in clinical trials. Nevertheless, most of the molecules tested so far are indole and sulfonic derivatives and therefore it is important to explore new classes of compounds, which might be useful in AD's pharmacotherapy [13]. Additionally, it is worth noting that only antagonists have been evaluated in clinical trials, thus searching for novel, potent 5-HT₆R agonists with beneficial pharmacokinetic profile seems to be in high priority.

Our group designed novel 1,3,5-triazine-based derivatives exhibiting high affinity and selectivity towards the 5-HT₆R. Considering the non-indole and non-sulfone nature of the newly discovered compounds, this approach opened new possibilities in searching for rational strategy in the treatment of CNS diseases. Excitedly, several active 5-HT₆R

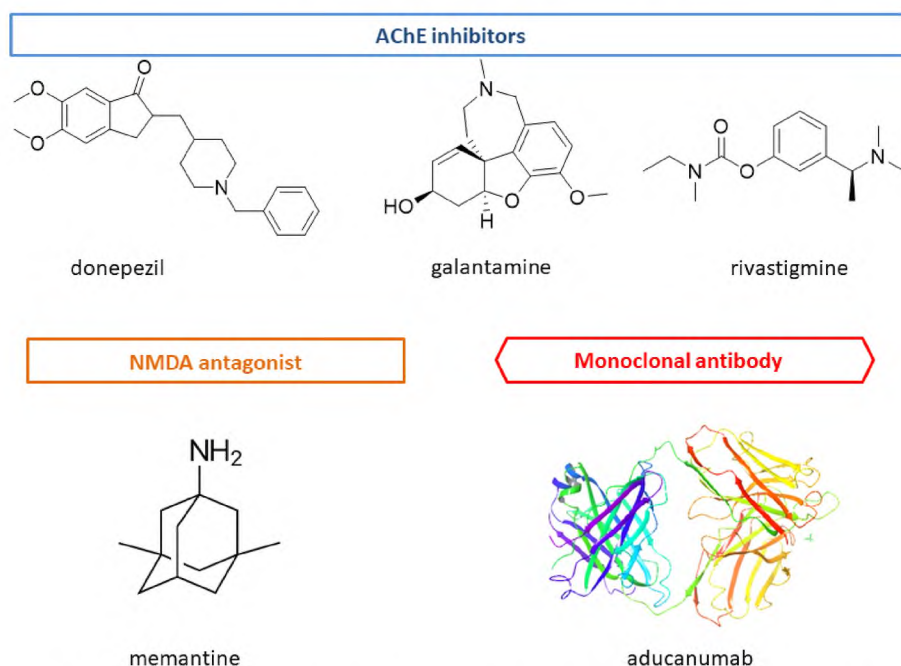


Fig. 1. Currently available treatments for Alzheimer's disease - synthetic and biological drugs.

triazine derivatives have already shown significant procognitive effects in the Novel Object Recognition (NOR) test in rats [14]. In the light of our previous research, the deep structure-activity relationship analysis has been performed proving that the topology of the alkyl linker and the substitution mode of chlorine atoms in the aromatic ring are of particular importance in terms of the 5-HT₆R affinity [15]. However, all the already tested triazine-based compounds were confirmed 5-HT₆R antagonists. Taking into account that even small structural change may influence the functional activity, we designed a novel series including two main chemical modifications (Fig. 2).

As very efficient procedures in rational drug design base on bioisosterism, and one of the most useful modifications in medicinal chemistry is the replacement of oxygen atom with the sulfur one also coming from the chalcogen family [16–18], we synthesized a series of S-containing triazine derivatives (Fig. 2). On the surface, these two mentioned atoms have nearly identical chemical and physical properties, but in fact small differences can lead to major changes in interaction of a molecule with a biological target [19]. The main differences that seem to matter the most are size, electronegativity, polarizability, and redox properties [20] (Fig. 3). These features become apparent in type and strength of the formed interactions, such as hydrogen bonds and σ -hole interactions [21].

All the information presented above and the fact that sulfur is indeed one of the most important atoms in the chemical composition of FDA-approved drugs encouraged us to synthesize a series of analogues, which contain a sulfur atom instead of oxygen in the linker (14–30 vs. 1–13, Fig. 2).

Moreover, our previous metabolic studies using rats' liver microsomes showed that the most active compounds are metabolized mainly into *N*-demethylated products [15,23]. As the metabolites can feature with different biological properties, it is always important to synthesize them and compare their properties with parent compounds. Hence, herein presented series was additionally enriched with also newly synthesized, five derivatives after *N*-demethylation reaction (modification 2, Fig. 2.).

In summary, the changes in the designed and synthesized compounds involve as many as four sites, of which this paper mainly investigated the biological effect of the sulfur atom and the removal of the methyl group from piperazine. In this work, we present the synthesis and biological evaluation of 18 new 1,3,5-triazine derivatives. For the whole series, the affinity towards the 5-HT₆R and enzymatic activity towards AChE and BChE were determined. Selected compounds have been evaluated in extended pharmacological screening, including functional assays to assess their mode of action towards 5-HT₆R. The research was enriched with a deeper structural insight, including X-ray crystallographic analysis for two compounds and the molecular modelling support in term to explain the different functional modes of action for respective O- and S-ether compounds. For representative compounds, ADME-Tox properties



	3.44	Electronegativity	2.58	
	0.66	Covalent radius (Å°)	1.05	
	1.52	van der Waals radii (Å°)	1.80	

Fig. 3. Comparison of selected physicochemical properties of oxygen and sulfur [14,22].

in vitro have been determined. Moreover, one selected active 5-HT₆R agonist was examined in behavioural tests *in vivo* in order to evaluate its procognitive, anxiolytic- and antidepressant-like effects in rats. At the end, a comprehensive structure-activity relationship analysis and potential CNS penetration for the investigated compounds have been discussed.

2. Results

2.1. Chemistry

2.1.1. Synthesis

The final compounds were obtained by three- or four-step synthesis (Scheme 1). The first step involved the Williamson synthesis of aromatic ethers 32–44 by reaction of the appropriate phenol or thiol derivative with the corresponding bromoester, based on the methods described earlier [15,24,25]. The subsequent move was the cyclic condensation of the previously obtained 4-methylpiperazin-1-yl biguanide dihydrochloride 32 with proper ester resulting in compounds 13–30. The replacement of sulfur with oxygen did not affect the first step of the reaction, but significantly hindered the cyclization, which is reflected in the yields of the final compounds. However, the most difficult modification was the removal of the methyl group, which tolerates a wide variety of reaction conditions. The first attempt was to try to introduce an acetyl group instead of a methyl group in the piperazine moiety, which was supposed to facilitate its hydrolysis to free piperazine in the last step. The reaction did not take place at the first stage of 4-acetyl-piperazin-1-yl biguanide dihydrochloride formation. Finally, compounds 26–30 were obtained by demethylation reaction using 1-chloroethyl chloroformate. The reaction mechanism is based on the nucleophilic attack of a tertiary amine on a chloroformate ester to form a carbamate intermediate via a quaternary ammonium salt species and loss of methyl chloride [26]. After hydrolysis of the carbamate in methanol, the required secondary amines were received. All final compounds 13–30 were obtained as racemic mixtures. Additional chemical data are provided in Supplementary Information.

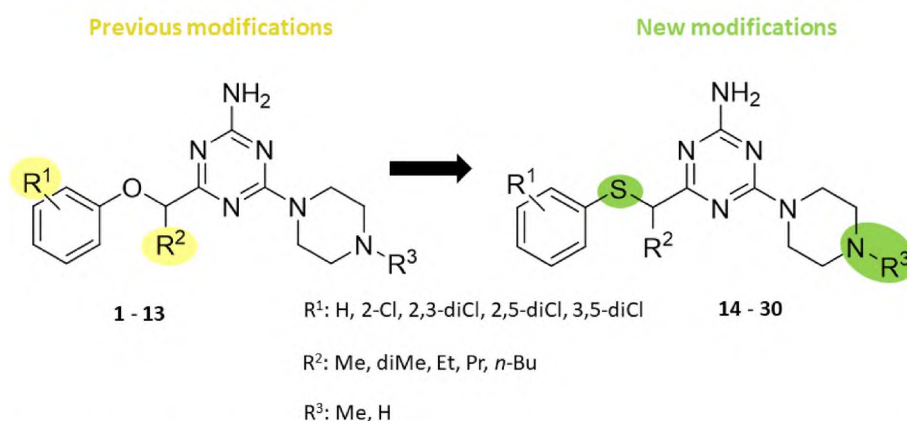
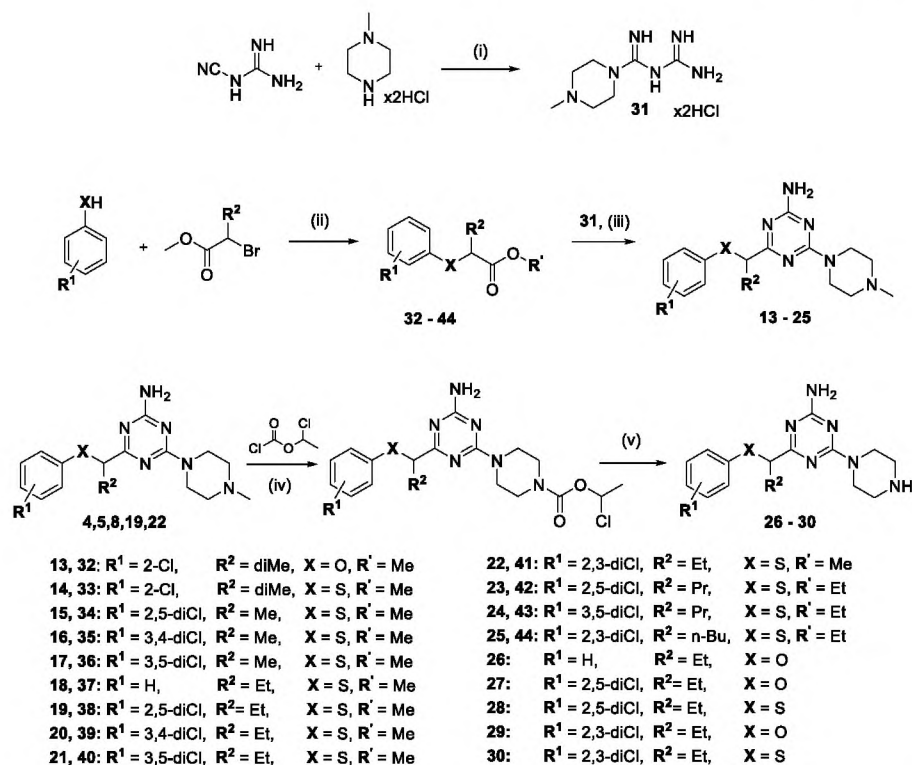


Fig. 2. Chemical modifications introduced in the earlier (compounds 1–13) and present (compounds 14–30) studies.



Scheme 1. Synthetic route for compounds 13–30. Reagents and conditions: (i) BuOH, reflux, 16 h; (ii) acetonitrile, K₂CO₃, reflux, 1–16 h; (iii) absolute methanol, Na, reflux 24 h, Y = 21–53%; (iv) 1-chloroethyl chloroformate, DCE, TEA, reflux 24 h; (v) MeOH, reflux 24 h, Y = 2–70%.

2.1.2. Crystallographic analysis

The molecular geometries of the **1** and **19** in the crystals with the atom-numbering scheme are presented in Fig. 4.

The triazine ring of **19** is more planar than **1**, with r.m.s. deviations of the fitted atoms of 0.0089 Å and 0.0251 Å, for **19** and **1**, respectively. The piperazine ring adopts chair conformation with equatorial position of the methyl group. The substituent at the N2 atom is not in a typical equatorial position with a torsion angle C4–N2–C7–C8 of about 180°. The value of this angle, being 151.2(3) for **19** and 98.7(1)° for **1**, suggests position closer to axial for **1**. The interplanar angle between triazine and piperazine rings is 8.9(2) and 59.23(5)°, while between triazine and aromatic rings is 81.92(8) and 84.12(6)°, for **19** and **1**, respectively. Thus, the triazine and piperazine rings are almost coplanar in the crystal structure of **19** (Fig. 5). Such mutual arrangement of the triazine and piperazine rings we have noticed for the first time. In the determined crystal structures containing the 4-(4'-methylpiperazin-1'-yl)-1,3,5-triazine moiety, we have observed the higher values of this angle, namely 43.30(5)° and 28.65(5)° [15]. It is worth noting, that geometry of molecules containing oxygen atom in the different linker is very similar, whereas the geometry of molecule containing in the linker sulfur atom in comparison to the molecule with oxygen atom shows big differences (Fig. 5).

The intermolecular interactions in the crystal structure of **19** are dominated by the O–H...N and N–H...O intermolecular hydrogen bonds. Molecules of propan-1-ol are engaged in these interactions (Fig. 6b). The other interactions are noticed in the crystal structure of **1** (Fig. 6a). In this structure, the main motif of intermolecular interactions is based on N–H...N hydrogen bonds, similar to other crystal structures determined earlier [15].

2.2. Pharmacological screening

2.2.1. 5-HT₆R and GPCRs

2.2.1.1. Radioligand binding assays (RBA) in vitro. All new triazine-based components (**13–30**) were subjected to radioligand binding assays to determine their affinity for 5-HT₆, 5-HT_{2A}, 5-HT₇ serotonin receptors and dopaminergic D₂. Results are presented in Table 1.

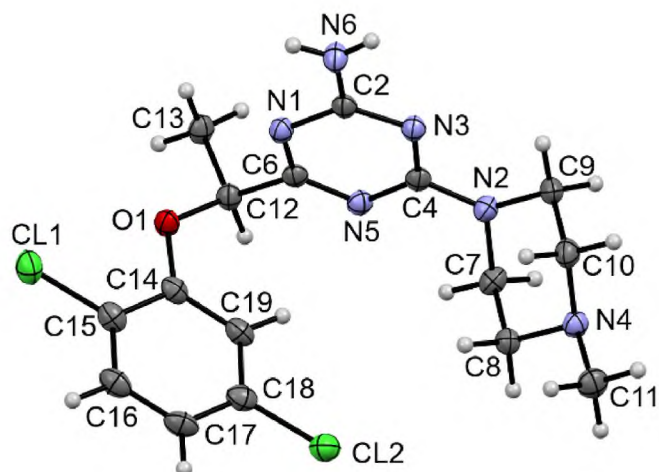
This study focuses on investigation of the biological effects induced by the interactions of the synthesized compounds with the 5-HT₆ receptor. Affinities with other competing targets (5-HT_{2AR}, 5-HT_{7R}, D₂R) were also identified to exclude their potential impact as many 5-HT_{2AR} and 5-HT_{7R} ligands display antidepressant-like activities [27,28]. Furthermore, some studies identify 5-HT_{2AR} and D₂R as important targets for the treatment of memory impairments and cognitive function disorders [29–31].

In similarity to the previously tested compounds **1–12**, new compounds **13–30** showed significant submicromolar affinities for 5-HT₆R (K_i: 5–476 nM) and distinct selectivity over 5-HT_{7R}. The most active ones: **19** and **23** displayed the 5-HT₆R affinity in the range of olanzapine but were much more selective over the tested off-targets. The highly active agent **27** and the moderate ones: **25**, **29** and **30** were found dual 5-HT₆R and 5-HT_{2AR} ligands with corresponding K_i values < 200 nM for both the targets.

Interestingly, among S-analogues (**18**, **19**, **22**) of the most active O-ether 5-HT₆R agents (**4**, **5**, **8**), only compound **19** kept the same affinity range (as **5**), being the most potent within the whole series **1–30**. Thus, compound **19** was selected for all steps of the extended screening planned in this work.

2.2.1.2. Functional studies in vitro. Selected active 5-HT₆R ligands (**19**, **22**, **27**, **28**, and **30**) were further evaluated for their intrinsic activity in functional assays in order to characterize their mode of action towards 5-HT₆R. The experiment included measurement of cAMP accumulation

a)



b)

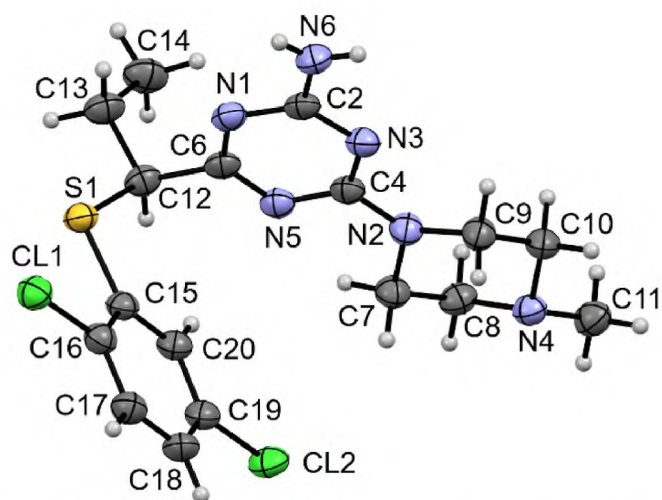


Fig. 4. The molecular geometries of (a) **1** and (b) **19** in the crystals showing the atom-numbering scheme. Displacement ellipsoids are drawn at the 50% probability level.

in 1321N1 cells (Table 2).

The results indicate that all tested sulfur compounds (**19**, **22**, **28**, **30**) turned out to be agonists with moderate potency. Interestingly, these compounds are the first characterized 5-HT₆ receptor agonists found among the 1,3,5-triazine compounds. All compounds from this chemical group previously studied by our team, including the direct oxygen analogues of compounds **19**, **22**, **28**, **30** showed antagonistic mode of action [15,23–25,32,33].

2.2.2. Inhibition assays of cholinesterases ligands

As widely reported, both acetyl- (AChE), and butyryl- (BChE) cholinesterase exhibit several functions in relation to AD pathophysiology, representing reversible (galantamine and donepezil), as well as pseudo-irreversible (rivastigmine) AChE inhibitors, the only approved drugs for the symptomatic treatment of mild-to-moderate AD, in association with the N-methyl-D-aspartate receptor antagonist memantine. These drugs contribute to regulate level of the neurotransmitter

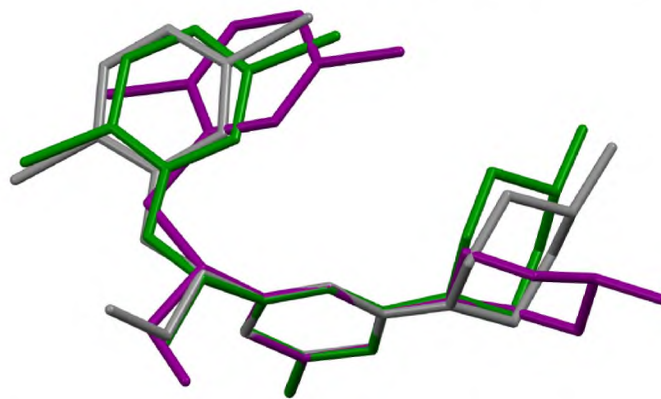
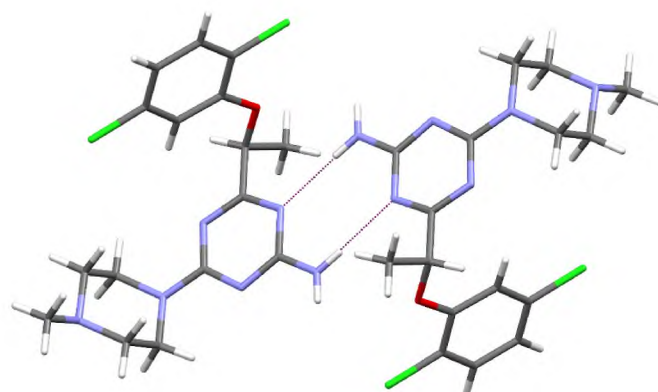


Fig. 5. The overlap of the triazine rings of **1** (green), **19** (purple) and the oxygen analogue of **19** for which the crystal structure was published earlier [15]. H atoms have been omitted for clarity.

a)



b)

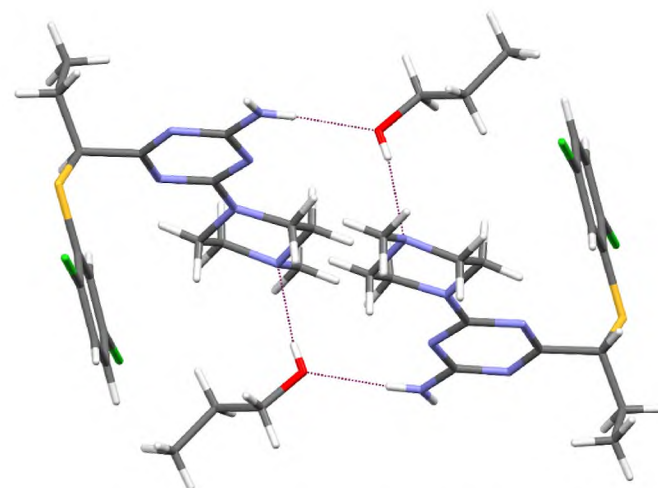
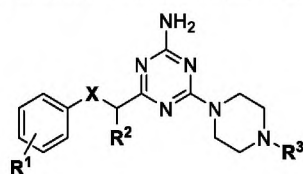


Fig. 6. The intermolecular interactions of two molecules (a) **1** and (b) **19**. Dashed lines indicates the intermolecular hydrogen bonds. The disordered molecule of propan-1-ol is depicted only for major occupancy.

acetylcholine (ACh) into hippocampus, and into the whole brain cortex, which are related to cognitive and memory impairment and decline [34, 35]. Aiming to exploit their potential as multitarget compounds, the whole series of triazine-based components (**1–30**) have been tested also

Table 3
Percentage of inhibition and half maximal concentration (IC₅₀) values of *ee*AChE and *hs*BChE of derivatives 1–30.



No	R ¹	R ²	X	R ³	AChE ^{a,c} inhibition % at 10 μM	AChE IC ₅₀ (μM) ^{b,c}	BChE ^{a,d} inhibition % at 10 μM	BChE IC ₅₀ (μM) ^{b,d}
1	2,5-diCl	Me	O	Me	39 ± 4	–	not active	–
2	3,4-diCl	Me	O	Me	52 ± 5	9.52 ± 0.10	4 ± 3	–
3	3,5-diCl	Me	O	Me	71 ± 13	3.95 ± 0.16	2 ± 2	–
4	H	Et	O	Me	21 ± 4	–	not active	–
5	2,5-diCl	Et	O	Me	53 ± 10	11.2 ± 0.18	2 ± 2	–
6	3,4-diCl	Et	O	Me	21 ± 8	–	not active	–
7	3,5-diCl	Et	O	Me	40 ± 5	–	not active	–
8	2,3-diCl	Et	O	Me	12 ± 6	–	10 ± 3	–
9	2,5-diCl	Pr	O	Me	17 ± 8	–	15 ± 3	–
10	3,5-diCl	Pr	O	Me	46 ± 6	–	not active	–
11	2,3-diCl	Pr	O	Me	26 ± 10	–	11 ± 7	–
12	2,3-diCl	n-Bu	O	Me	15 ± 5	–	93 ± 7	0.50 ± 0.10
13	2-Cl	diMe	O	Me	31 ± 8	–	22 ± 1	–
14	2-Cl	diMe	S	Me	23 ± 5	–	15 ± 1	–
15	2,5-diCl	Me	S	Me	52 ± 12	9.19 ± 0.10	2 ± 2	–
16	3,4-diCl	Me	S	Me	45 ± 2	–	12 ± 10	–
17	3,5-diCl	Me	S	Me	75 ± 8	5.37 ± 0.77	20 ± 10	–
18	H	Et	S	Me	20 ± 4	–	27 ± 2	–
19	2,5-diCl	Et	S	Me	21 ± 2	–	47 ± 7	12.10 ± 0.55
20	3,4-diCl	Et	S	Me	92 ± 8	4.57 ± 0.13	43 ± 2	15.00 ± 0.20
21	3,5-diCl	Et	S	Me	24 ± 2	–	51 ± 8	9.80 ± 0.15
22	2,3-diCl	Et	S	Me	25 ± 4	–	17 ± 10	–
23	2,5-diCl	Pr	S	Me	34 ± 6	–	8 ± 3	–
24	3,5-diCl	Pr	S	Me	17 ± 3	–	23 ± 3	–
25	2,3-diCl	n-Bu	S	Me	9 ± 2	–	50 ± 7	9.95 ± 0.20
26	H	Et	O	H	22 ± 6	–	19 ± 3	–
27	2,5-diCl	Et	O	H	26 ± 5	–	41 ± 7	–
28	2,5-diCl	Et	S	H	25 ± 1	–	23 ± 2	–
29	2,3-diCl	Et	O	H	23 ± 3	–	50 ± 5	10.0 ± 0.11
30	2,3-diCl	Et	S	H	20 ± 10	–	31 ± 7	–
	Donepezil ^e	–	–	–	–	0.021 ± 0.020	–	2.75 ± 0.20
	Tacrine ^e	–	–	–	–	0.300 ± 0.050	–	0.025 ± 0.002

^a inhibition percentage at 10 μM concentration. Data are means ± SD of three independent measurements.

^b IC₅₀ values determined by interpolation of the sigmoidal dose-response curves as obtained by regression with GraphPad Prism software (ver. 5.01) of at least seven different data points. Data are means ± SD of three independent measurements.

^c Electric eel acetylcholinesterase.

^d Horse serum butyrylcholinesterase.

^e Donepezil and Tacrine were used as positive controls against AChE and BChE, respectively.

agents described [15,23–25,33], two pair of active representatives, with corresponding structures and a different heteroatom within linkers, i.e. O- (**5**, **27**) and S-ether (**19**, **28**), respectively, were selected for advanced molecular modelling studies. Results are shown in Fig. 7 (**5** vs. **19**) and in Supplementary Information (Fig. S10) (**27** vs. **28**).

The binding mode of compounds **5** and **19** was consistent with our previous study on different groups of 5-HT₆R ligands [15,24,25]. The protonated piperazine moiety formed a salt bridge with D3x32, and the 1,3,5-triazine fragment created a CH...π interaction with F6x51 and a hydrogen bond with T5x461. The terminal substituted phenyl ring fitted into a hydrophobic cavity formed by transmembrane domains (TMs) 3–5 and extracellular loop 2 (ECL2).

However, the only analysis of the binding modes obtained by the induced fit docking (IFD) did not explain the different pharmacological profiles of compounds **5** and **19**. Therefore, a series of 100 ns-long molecular dynamics (MD) simulations were performed using geometries selected by the IFD analysis. Next, MD trajectories were clustered (Fig. 7A), and the five most populated geometries were used to further analysis. The MD results indicated that **5** and **19** retained key L–R interactions (i.e. D3x32, F6x51, and T5x461) but significantly changed the receptor conformation (Fig. 7 B–C). What is interesting, only for **19**

halogen bond with the carbonyl oxygen of A4x56 was formed, and showed high stability during the whole MD simulations (average XB distance = 3.71 Å; σ-hole = 149 deg., compared to **5**: 4.91 Å and 137 deg., respectively).

Calculated changes at the position of geometric centers of individual amino acids showed significant differences between the conformations of **5** and **19** complexes (Fig. 7A). The largest changes (above 2 Å) within the binding pocket (areas marked in pink on the graphs of the individual helices) are visible in TMs 4–6, while changes did not exceed 2 Å in the other TMs (except for five amino acids of TM 2, which has no direct interaction with the ligands).

To explore the hypothesis that the potential source of the differences between the MD simulations for the complexes of **5** and **19** can be induced by internal preferences of the ligand structures, quantum mechanical calculations were performed. A non-covalent interaction (NCI) approach was used both for geometries of **5** and **19**, which came from single molecule geometry optimization and MD trajectory clustering. The isosurfaces of the reduced density gradient s(r) were examined, and the resulting plots were generated (Fig. 7D). Within both sources of structures of **19**, attractive non-covalent interactions were indicated which stabilized the in-plane orientation of 1,3,5-triazine and

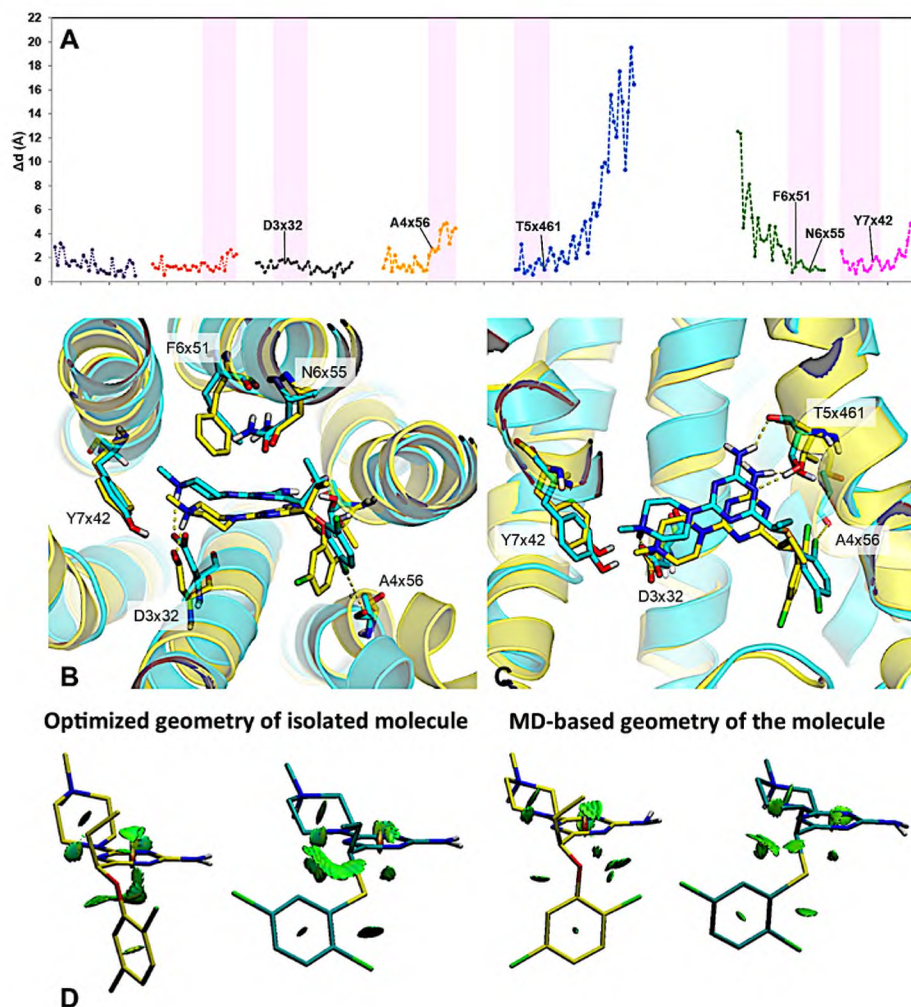


Fig. 7. (A) Plot illustrating the relationship between the position of the geometric center of a given amino acid, calculated as the mean difference between conformations of **5** and **19** selected from MD trajectory clustering. Additionally, fragments of the sequence of a given helix are marked by the pink area to determine the amino acids that form the receptor's binding site. (B–C) Comparison of **5** (yellow) and **19** (cyan) binding modes to the most populated conformation of 5-HT₆R obtained from the clustering of the MD trajectory. (D) Illustration of the intramolecular interactions via the gradient isosurfaces for the **5** and compound **19** – calculations performed separately for conformations obtained on single molecule geometry optimization and fetched from the most populated MD cluster.

substituted phenyl rings and improves the possibility to form a halogen bond with A4x56. Such intramolecular S...N chalcogen bond limits the compound's flexibility during MD simulations, which further probably causes a deviation of helices 4–5. Furthermore, exchanging sulfur to oxygen excludes the possibility of creating any intramolecular chalcogen bond, thus, the most populated conformation of **5** shows a twisting of the 1,3,5-triazine ring against the substituted phenyl plane.

The similar trends to those of pair **5** and **19** were also demonstrated by their demethylated analogues **27** and **28** (see SI, Fig. S10).

2.3.2. Molecular modelling to cholinesterases

Some valuable indications arise also simulating dockings of **5** to the AChE active site. Although the compound did not result as the best AChE inhibitor modelling, this derivative was indeed performed since **5** is a 2,5-dichloro triazine endowing valuable 5-HT₆ activity, hence we decided to challenge the role of this chemical motif also with respect to AChE inhibiting. Furthermore, to ensure that chirality is not a molecular determinant for esterases binding and inhibition, dockings of both anti-podes was carried out (Fig. 8, Table 4).

As depicted in Fig. 8, both (R) and (S) enantiomer of **5** occupy quite the whole molecular surface guarding the available active center gorge of AChE, and thereafter enzyme binding is reinforced by several and different type of contacts: the charged piperazine nitrogen makes salt bridge with Glu202, the amine group embraces hydrogen bonds with the hydroxy of Tyr337 and Tyr341 with this latter residues producing also significant π - π stacking with the dichloro-substituted phenyl ring of the ligand, that is also recruiting the indole ring of the PAS Trp286.

Table 4

Docking scores for compound **5** to hAChE.

	FEB ^(a)	ΔE ^(b)	EFF ^(c)	TAN ^(d)	POP ^(e)
(R)- 5	-10.73	0.00	-0.413	0.703	29/100
(S)- 5	-9.91	0.92	-0.381	0.650	1/100
donepezil	-10.83	0.05	-0.387	1.279	470/100

^a FEB Free Energy of Binding.

^b ΔE Energy difference between the selected pose and the relative global minimum.

^c EFF Ligand efficacy.

^d TAN Tanimoto_Combo similarity coefficient of with donepezil X-ray pose.

^e POP Cluster members population.

With very particular interest, two halogen bond mediated aromatic contacts with Tyr72 and Phe297 are indeed gained, and moreover both (R) and (S) configurations direct the short alkyl chain in a small hydrophobic pocket comprising the aforementioned aromatic amino acids. As a proof of these ligands binding the docking scores filtered according to the ESP rule (see methods) suggest overall a good compactness of the enzyme-inhibitor complexes produced by these new triazines with AChE (Table 4).

On the other hand, a very interesting data was achieved in BChE assays since compound **12** resulted as valuable (IC₅₀ = 0.50 μ M) inhibitor suggesting, as expected, that bulkier substituents might be better accommodated in the more accessible BChE binding site. Indeed, as earlier reported, some critical differences in the composition and extent of the molecular surface of BChE active site occurs with respect to AChE,

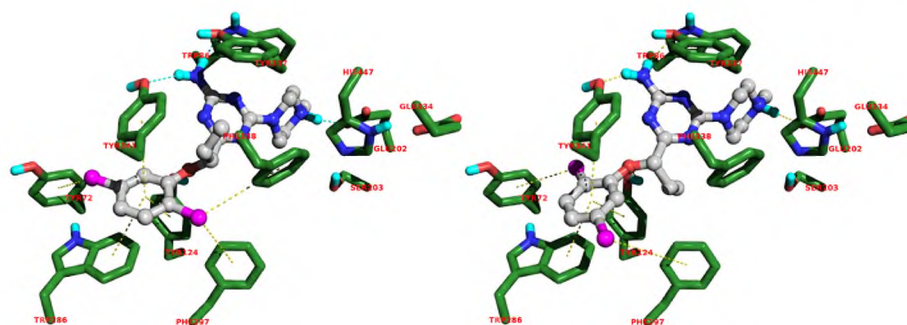


Fig. 8. Binding mode for (*R*)- (left) and (*S*)-5 (right) to the AChE active site. In the interaction pattern scheme to hydrogen bonds and π - π stackings are depicted in cyan and yellow respectively.

and this evidence is confirmed by more puckered binding conformation in ligand, mandatory for efficiently inhibition, as observed in several X-ray complexes including recent data referring to a potent BChE tacrine-methylanacardate hybrid inhibitor (TKN) [41], so dockings to the active site of this esterase was then investigated to acquire additional knowledge into the potential role of the triazine nucleus as efficient the esterase's inhibition.

As depicted in Fig. 9, compound **12** fits very well the inner part of the enzyme binding site being the nitrogen rich moiety of the ligand able to makes more than one hydrogen bond involving in the (*R*) stereocenter the Ser198 of the catalytic triad as well as the backbone of Trp82, while the (*S*) recruits with different interaction pattern Thr120 and Tyr332, suggesting good activity for both the configurations.

In addition, the dichloro aromatic pendant of the two enantiomers engages extensive π - π stackings with Trp231 and Phe239. As a matter of fact of the valuable submicromolar IC_{50} data, similar docking scores gained from the previously reported enantiomers of **5** were definitely observed for **12** (see Table 5).

2.4. ADMET *in vitro*

2.4.1. Metabolic stability

The most active compounds and their demethylated metabolites were examined in the metabolic stability assay. The study was performed using rat liver microsomes (RLMs). The test was carried out according to the procedure described previously [15,23,33]. The tested compounds (**19**, **22**, **28**, **30**) showed high metabolic stability, especially when compared to *O*-containing analogue of **22** which was

Table 5

Docking scores for compound **12** to BChE.

	FEB ^(a)	ΔE ^(b)	EFF ^(c)	TAN ^(d)	POP ^(e)
(<i>R</i>)-12	-9.04	0.00	-0.323	0.341	26/100
(<i>S</i>)-12	-9.25	0.00	-0.330	0.288	18/100
TKN	-8.09	0.50	-0.231	1.176	18/100

^a FEB Free Energy of Binding.

^b ΔE Energy difference between the selected pose and the relative global minimum.

^c EFF Ligand efficacy.

^d TAN Tanimoto_Combo similarity coefficient of with TKN X-ray pose.

^e POP Cluster members population.

biotransformed in more than 90% [15]. Successively, 91.62% of **28**; 86.77% of **30**; 74.87% of **19**; 69.12% of **22** remained in the reaction mixture (Table 6). Interestingly, the demethylated piperazine compounds (**28**, **30**) turned out more stable than their methylated analogues (**28** vs. **19** and **30** vs. **22**). Four metabolites were observed for **28** after incubation with RLMs, respectively five metabolites for **19** and six metabolites for both **22** and **30**. The main metabolites were formed by hydroxylation at piperazine ring and also aromatic moiety.

The most common metabolic reaction is hydroxylation, which was observed for all tested compounds. Mass spectra are included in the Supplementary Information (Fig. S1-Fig. S8).

2.4.2. Permeability Caco-2

The Caco-2 permeability assay is considered to be representative of human absorption *in vivo* as provides a good prediction for compounds

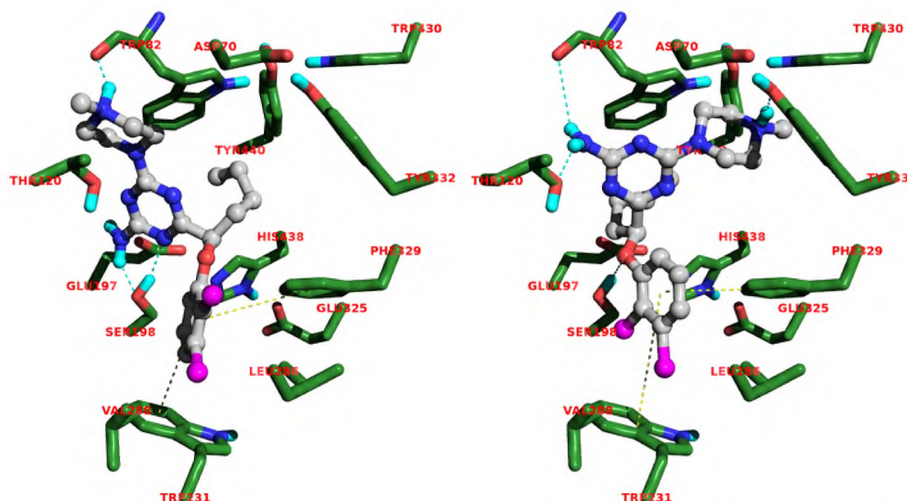


Fig. 9. Binding mode for (*R*)- (left) and (*S*)-12 (right) to the BChE active site. In the interaction pattern scheme to hydrogen bonds and π - π stackings are depicted in cyan and yellow respectively.

Table 6

The molecular masses, metabolic stability and metabolic pathways of examined compounds **19**, **22**, **28**, **30** and the reference drug Verapamil.

Substrate	Remaining of the substrate [%]	Number of metabolites	Metabolic pathway*
19	74.87	4	hydroxylation demethylation
22	69.12	5	Hydroxylation demethylation
28	91.62	2	hydroxylation double
		1	hydroxylation not identified
30	86.77	4	hydroxylation not identified
Verapamil	37.28	2	demethylation defragmentation

**Results revealed in previous studies, determined according to the same procedures [42].

* Estimated according to MS spectra supported by in silico data (see SI Fig S1-Fig. S8).

that display active uptake, efflux or pass through the membrane via the paracellular route. The transport across the cell monolayer in both directions (A-B and B-A) allows the determination of the efflux rate by the cell monolayer and provides an indicator of whether a compound is susceptible for the active efflux. The value of efflux ratio higher than 2 usually indicates involvement of apical efflux transporters [43]. Based on *in vitro/in vivo* correlation studies, the *Papp* values obtained from the Caco-2 assay predict the following range of *in vivo* absorption: a low permeability - $Papp < 5 \times 10^{-6}$ cm/s, and a high permeability - $Papp > 5 \times 10^{-6}$ cm/s [44]. As shown in Table 7, compound **22** has an excellent permeability in Caco-2 conditions with *Papp* value 56.7 ± 8.2 for A-B direction, and *Papp* value 92.6 ± 16.7 for B-A direction might suggest that the compound **22** may be subjected to active efflux. Compound **19** has also excellent permeability (*Papp* value 35.4 ± 3.87 for A-B) and permeates only by passive diffusion.

2.4.3. Hepatotoxicity and neurotoxicity

The hepatotoxicity and neurotoxicity were determined in HepG2 and SH-SY5Y cell lines, respectively. The cell lines' growing conditions and the assay procedures were described previously [15,23,33]. The viability of cells after 72 h of incubation with compounds was estimated by standard MTS procedure and showed no differences between toxicity of **19**, **22**, **28**, **30** against hepatoma and neuroblastoma cell lines (Fig. 10A and B). The highest, statistically significant effect was observed only in the highest doses 50 and 100 μ M. Doxorubicin (DX, 1 μ M) was used in both assays as the reference cytostatic drug.

2.4.4. Neuroprotection - antioxidant action

The antioxidant activity of the final compounds (**5**, **12**, **19**, **22**, **26**, **28**) was evaluated *in vitro* using the 2',7'-dichlorodihydrofluorescein diacetate (DCFH-DA) cell-based assay. The test consisted of measuring

Table 7

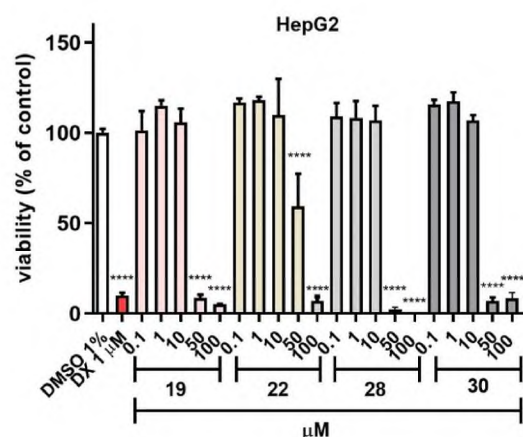
The results obtained in a bidirectional Caco-2 permeability assay for compounds **19**, **22** and the reference caffeine (CFN).

Cpd	^a <i>Papp</i> (10^{-6} cm/s) \pm SD		^b Efflux ratio
	A-B	B-A	
CFN	15.6 \pm 0.55	17.9 \pm 1.9	1.14
19	35.4 \pm 3.87	77.9 \pm 11.8	2.22
22	56.7 \pm 8.2	92.6 \pm 16.7	1.63

^a *Papp*, apparent permeability coefficient, test permeability for each compound was tested in triplicate, data are mean \pm standard deviation (SD).

^b the quotient of the mean *Papp* for B-A to the mean *Papp* for A-B [43].

A



B

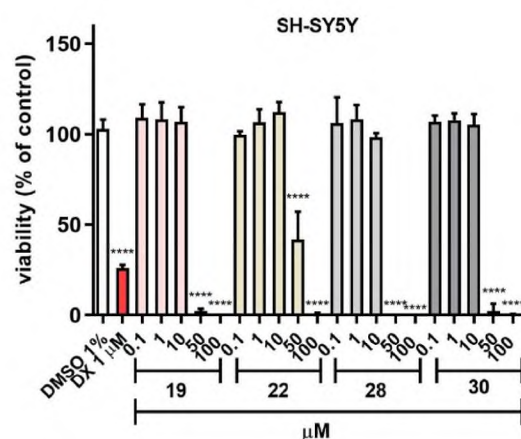


Fig. 10. The effect of cytostatic drug doxorubicin (DX) and **19**, **22**, **28**, **30** on hepatoma HepG2 (A) and neuroblastoma SH-SY5Y (B) cell lines' viability after 72 h of incubation at 37°, 5% CO₂. The statistical significance (GraphPad Prism 8.0.1) was evaluated by a one-way ANOVA, followed by Bonferroni's Comparison Test (****p < 0.0001 compared with negative control DMSO 1% in growth media).

the reducing effect of the selected compound against oxidation of 2',7'-dichlorodihydrofluorescein (DCFH) to the fluorescent probe 2',7'-dichlorofluorescein (DCF). Two different cell types were used to study protection against oxidative effects. Human hepatocellular carcinoma (HepG2) cells were chosen as the first model because of their increased oxidative metabolism, which causes cellular oxidative stress and/or generates reactive metabolites. Thus, it may be assumed that HepG2 cells are suited to study protection against oxidative and cytotoxic effects, if any [45]. Furthermore, neuroblastoma SH-SY5Y cells have been used as a model for human neurons. Quercetin, a naturally occurring compound known to have strong antioxidant activity, has been used as positive control. The results are summarized in Table 8.

Compound **5** showed a notable antioxidant activity on HepG2 cells with an IC₅₀ value of 7.4 ± 1.0 μ M, that is slightly lower than that of quercetin, while being less active on SH-SY5Y cell line (IC₅₀ = 81.3 ± 0.5 μ M). A dramatic loss of activity was observed in the thio-isoster of **5**, compound **19**, that is not active toward both the cell lines. A similar behaviour was observed for the 2,3-dichloro analogue of **19**, compound

Table 8

Antioxidant potencies in the DCFH-DA cell-based assay for compounds **5**, **12**, **19**, **22**, **26**, **28** and quercetin.

Compound	IC ₅₀ ± SEM [μM] ^[a]	
	HepG2	SH-SY5Y
5	7.4 ± 1.0	81.3 ± 0.5
12	13.2 ± 0.8	29.9 ± 0.4
19	>100	>100
22	>100	>100
26	0.02 ± 0.01	42.1 ± 0.2
28	0.052 ± 0.02	55.8 ± 1.2
Quercetin	12.5 ± 0.4	5.6 ± 0.4

^a Values are the mean of at least three determinations performed in triplicate.

22, that was not able to reduce the H₂O₂-induced oxidation in both cell lines. Interestingly, this trend was reverted in the *N*-demethylated analogue of **19**, compound **28**, that showed a remarkable antioxidant activity particularly on HepG2 cells with an IC₅₀ in the nanomolar range (0.052 ± 0.020 μM). Among the tested compounds, the most impressive activity was observed for the *N*-demethylated *O*-containing analogue **26** towards the same cell line with an IC₅₀ value of 0.02 ± 0.01. Both compounds, **26** and **28** showed a moderate activity on SH-SY5Y cell.

2.4.5. Antiplatelet activity *in vitro*

Apart from the potent affinity for 5-HT₆R, compound **19** represents the moderate 1,3,5-triazine 5-HT_{2A}R agent. As blood platelets express 5-HT_{2A} receptors and the 1,3,5-triazine scaffold occur in compounds promoting the platelets aggregation [46], we aimed to evaluate the influence of compound **19** on platelet aggregation. Blockade of platelet 5-HT_{2A} receptors decreases of intracellular Ca²⁺ levels and consequently causes the inhibition of platelet activation and aggregation [47]. Indeed, compound **19** inhibited platelet aggregation dose-dependently, as shown in Fig. 11., giving an IC₅₀ value of 73.4 ± 13.7 μM. For comparison, aspirin inhibited platelet with IC₅₀ value of 17.4 ± 4.0 μM. On that basis we can state that compound **19**, showed a favorable safety profile, as it did not potentiate platelet aggregation induced by collagen. Contrary, it exerted moderate antiplatelet effect, four times weaker than aspirin.

2.5. Behavioral studies

Based on *in vitro* studies, compound **19** was selected for *in vivo* studies. In the first step of behavioral studies, the ability of compound **19** to impact and/or reverse memory impairment in the NOR test was investigated. The NOR test was chosen based on our previous studies with 5-HT₆ receptor triazine antagonists [23] as well as the knowledge

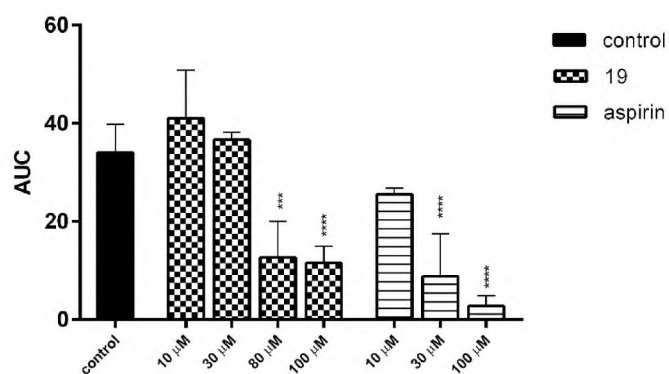


Fig. 11. Effects of compound **19** on *in vitro* whole rat blood aggregation induced by collagen (1.6 μg/mL). Results are expressed as mean ± Δ/2, where Δ is a width of the 95% confidence interval (CI); n = 3–6; ***p < 0.001, ****p < 0.0001 (statistical analysis: one-way ANOVA; post hoc Dunnett test). AUC: area under the curve. Aspirin used as reference.

that various other 5-HT₆ receptor agents are capable of reversing memory impairments induced by scopolamine, dizocilpine (MK-801) or ketamine [48,49]. We decided to assess the ability of the 5-HT₆R agonist **19**, to reverse MK-801-induced memory impairment, considering that this NMDA receptor antagonist induces memory deficits in rodents, related to different human cognitive disturbances, which can be observed in dementia [50] and schizophrenia [51], both. The preference of rats to explore the novel object rather than the familiar object in the T2 session denotes the ability of the investigated compound, given jointly with 0.1 mg/kg of MK-801, to reverse MK-801-induced memory impairment in the NOR test. To give thought to rats' preference of novel object exploration, the discrimination index (DI) was used (Fig. 12). Compound **19** administered at a dose of 0.3 mg/kg reversed MK-801-induced memory impairments, but this result did not reach statistical significance; however, DI observed for this dose of **19** was like the vehicle-treated group of animals. Higher doses of **19** (1 and 3 mg/kg) were total inactive in this test (Fig. 12).

Compound **19** did not improve the recognition memory of rats after alone administration at the broad dose range of 0.3–10 mg/kg in the NOR test but also simultaneously it did not induce memory impairments (Fig. 13).

Simultaneously with the evaluation of DI in the T2 phase in the NOR test, the total exploratory time of objects in the recognition phase (T2) was measured after *i.p.* administration of compound **19** alone and jointly with MK-801, to assess the impact of the injected compounds on the exploratory activity of rats. Compound **19** injected alone (at the dose range 0.3–10 mg/kg) or jointly (at the dose range 0.3–3 mg/kg) with MK-801 (0.1 mg/kg), did not change total exploratory activity in T2 (Table 9). Therefore, the observed lack of impact of the studied **19** on memory processes, both natural and disturbed (Figs. 12 and 13) was not related to, for example, hyperlocomotor activity measured in T2 session.

As a next step, we assessed the antidepressant- and anxiolytic-like properties of compound **19** in the forced swim (FST) and the elevated plus maze (EPM) tests, respectively. Some antidepressant-like activity was observed only for compound **19** given at the highest dose (10 mg/kg). In this dose, the immobility reduction by approximately 30% versus the vehicle treated group was statistically significant (p < 0.001) (Fig. 14).

In the EPM test, compound **19** did not show anxiolytic-like properties

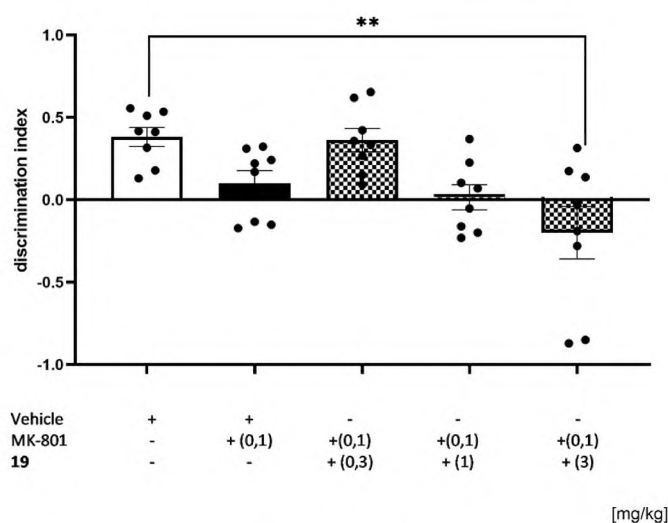


Fig. 12. The impact of compound **19** on MK-801-induced memory impairment in NOR test. Compound MK-801 was given *i.p.* 30 min while **19** was administered *i.p.* 60 min, before the T1 session. The observation of 8 rats was carried out for 3 min. The data are shown as the mean ± SEM of 8 rats, and were statistically evaluated by one-way ANOVA followed by Bonferroni's post-hoc test, **p < 0.01 vs. vehicle-treated group (one-way ANOVA for discrimination index (DI) for compound **19** in NOR test: F(4,35) = 6.6248, p < 0.001).

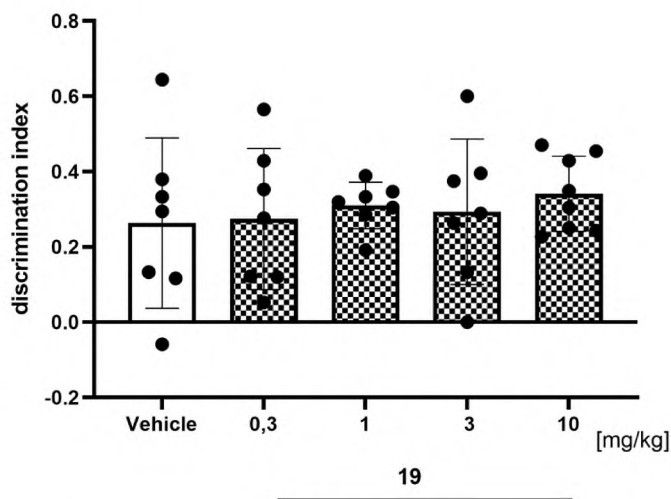


Fig. 13. Effect of compound **19** in NOR test in rats. Compound **19** was administered *i.p.* 60 min. before the T1 session. The rats were observed for 3 min. The data are presented as the mean \pm SEM of 7–8 rats. The data were statistically evaluated by one-way ANOVA followed by Bonferroni's post-hoc test (one-way ANOVA for discrimination index for compound **19** in NOR test: $F(4,32) = 0.5154$, NS). NS = not significant.

Table 9

The effect of compound **19** on the exploration activity of rats in the NOR test.

Treatment	^a Dose [mg/kg]	Total exploratory time in T2 session [s]
Vehicle	0	34.63 \pm 4.93
MK-801 + vehicle	0.1 + 0	48.88 \pm 5.40
19 + MK-801	0.3 + 0.1	45.00 \pm 5.15
	1 + 0.1	36.38 \pm 6.51
	3 + 0.1	40.63 \pm 3.94
		$F(4, 35) = 1.2699$; NS
vehicle	0 + 0	31.43 \pm 4.36
19	0.3	38.43 \pm 4.57
	1	45.43 \pm 1.89
	3	28.50 \pm 4.90
	10	34.50 \pm 4.36
		$F(4,32) = 2.3913$; NS

^a Compound MK-801 was given *i.p.* 30 min while **19** was administered *i.p.* 120 min, before the T2 session. The observation of rats was carried out for 3 min. The data are shown as the mean \pm SEM of 8 rats, and was statistically evaluated by one-way ANOVA followed by Bonferroni's post-hoc test.

in the entire range of doses used (0.3, 1 and 3 mg/kg) (see SI Tab. S3). Administration of compound **19** did not also change the total exploratory activity measured simultaneously with the anxiolytic activity (see SI Tab. S5).

All parameters presented in Table S4 (SI) describe the exploratory activity of rats that were measured using the automated version of the EPM, simultaneously with the anxiolytic-like activity. There were no significant effects observed for compound **19** in the whole dose range used (see SI, Table S3).

The results obtained in this study are preliminary and are the starting point in the search of the pharmacological activity of 1,3,5-triazine 5-HT₆R ligands. Compound **19** has weak activity in the NOR test, did not present anxiolytic properties in EPM test, and showed antidepressant action in FST at the highest dose used. Carried out studies with this compound are in line with literature data which demonstrated that 5-HT₆R stimulation with an agonist does not lead to the impairment of cognitive processes [48,52]. Modulation of 5-HT₆R function has been shown to exert promising effects on memory and learning processes in rodent's models of amnesia. Especially 5-HT₆R antagonists improved learning and/or memory processes in such preclinical tasks as: NOR test,

social recognition task, Morris Water Maze [53–56] as well as prevented memory disturbances induced by scopolamine [57,58], phencyclidine [59] or MK-801 [48]. The behavioral results obtained for compound **19** demonstrate weak activity of this triazine 5-HT₆R agonist as a potential memory enhancer than previously reported ability to reverse MK-801-induced memory impairments for triazine 5-HT₆R antagonists [15,23,24,60]. However such results also give some light on the further chemical modifications in the search for compounds that could improve the symptoms of AD.

3. Discussion

3.1. Qualitative SAR trends

The two main structural modifications performed for the newly presented series were addressed in order to analyze an influence on the affinity for 5-HT₆R and concerned: (i) exchange of oxygen to sulfur in the linker, (ii) presence vs absence of methyl group on piperazine moiety. The ChEs screening performed for the whole series gives also opportunity to search for trends in structure-ChEs inhibitory properties relationship, for AChE and BChE, respectively. Simultaneously, these chemical changes were aimed at improving the pharmacological profile and ADME-Tox properties of the new derivatives. The results acquired from this research allow for a complex overview of the qualitative structure-activity relationship.

The new compound library presented here contains 18 compounds, 16 of which showed high affinity for 5-HT₆R, with K_i values lower than 200 nM, 14 compounds have a sulfur atom in the linker, each with its oxygen analog for a better comparison. Replacement of these atoms did not result in drastic changes in binding for 5-HT₆R but a majority of sulfur analogues had a slightly lower affinity. However, it is immensely interesting to note that this small modification resulted in a change in intrinsic activity toward 5-HT₆R evaluated in functional assays. All tested sulfur compounds (**19**, **22**, **28**, **30**) appeared to be agonists in the nanomolar range, in contrast to their oxygen analogues, which are potent antagonists. This behaviour can be explained by the analysis of several molecular dynamics performed, which reveal conformational changes of the receptor depending on the docked S- or O- ligand, which consequently leads to a change in this mechanism of action. Of great importance here is the sulfur atom, which forms an intramolecular S...N chalcogen bond that rigidifies the molecule. These studies confirm that S-mediated chalcogen bonds like hydrogen bonds are common in chemical and biological systems and play an active role in structure and function.

Our previous studies show the effect of affinity of different types of substituents in the aromatic ring. In this work, we focus only on chlorine atoms as substituents and their position in the ring in the context of SAR analysis. The affinity assay results for 5-HT₆R indicate –2,5-diCl as the best position, followed by –2,3-diCl, –3,5-diCl and the worst for –3,4-diCl what is in line with our previous research in this group of compounds [15]. The main reason for this phenomenon, made evident by in silico studies, is the presence of different types of halogen bonds with amino acid residues of the receptor. The presence of chlorine atoms favorably affects the lipophilicity of the compounds, which in turn improves the penetration of membrane barriers, including the blood-brain barriers (BBB).

Concerning ChE inhibition, due to the paucity of significant data no structure activity relationship might be proposed for both types of the enzyme, even though some clues on the potential esterase's inhibition might be foresee. Indeed, compounds bearing a phenoxy group showed weak inhibition of both AChE and BChE, with exception of compound **3**, which exhibited a moderate AChE inhibition with IC_{50} value in the low micromolar range of concentration, and compound **12**, the only selective BChE inhibitor identified in the study, thus showing a sub-micromolar concentration IC_{50} value. Among the thiophenoxy congeners, compound **17** and **20** mainly returned a promising AChE

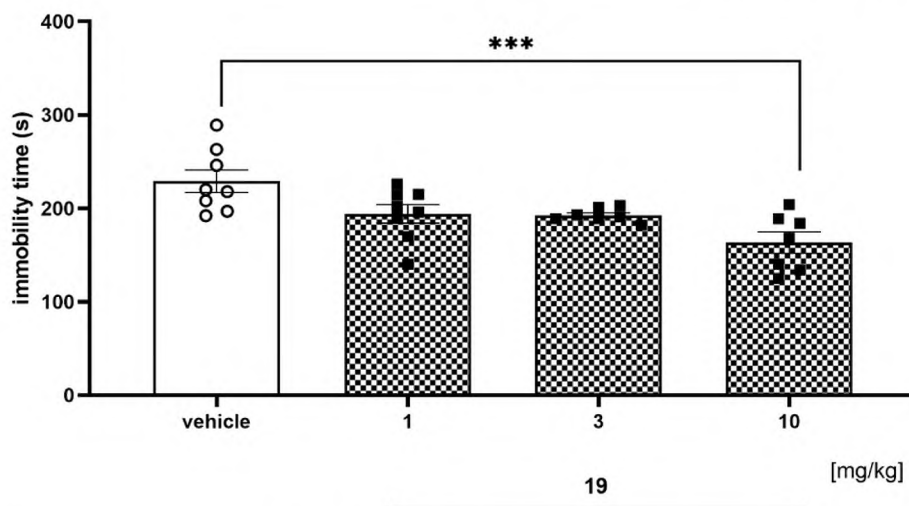


Fig. 14. Effect of compound 19 in FST in rats. Compound 19 was administered *i.p.* 60 min. before the test. The rats were observed for 5 min. The data are presented as the mean \pm SEM of 7–8 rats. The data were statistically evaluated by one-way ANOVA followed by Bonferroni's post-hoc test (one-way ANOVA for compound 19 in FST: $F(3,26) = 7.2595$, $p < 0.01$).

inhibition, whilst in general this series of compounds seems to mainly inhibit BChE. Regarding AChE inhibition, the ether linker affected activity in a lesser extent than chlorine substitution pattern, thus appearing 3,5-diCl and 3,4-diCl the preferred. In contrast, the bulk effect of substituents on chiral carbon exhibited a deep effect on AChE inhibition: the bulkier substituent reduced activity with the rank $\text{Me} > \text{Et} > \text{Pr}$ in O-ethers, which was confirmed in S-derivatives, with only exception of compound 20, bearing an ethyl substituent. Some of the sulfur containing triazine mainly returned a preferably inhibition of BChE, though the most interesting compound was an O-ether congener 12, bearing a butyl chain on chiral carbon atom. Although in a lesser extent than AChE inhibition, yet chlorine substitution pattern and alkyl side chain both affected anti BChE activity, mostly in oxygenated than in thioether derivatives. Likely, it was due to the larger volume of the BChE active site gorge. We conclude that compound 5, which differs from the high affinity and active 5-HT₆ triazine 19 only with respect to the substitution of the sulfur with an oxygen atom, showed an appreciable IC₅₀ value (11.2 μM) suggesting that this chemical cliché might retain the measured serotonergic profile but at the same time endows cholinesterase activity.

On the other hand, compounds containing N-methylpiperazine and their counterparts with unsubstituted piperazine moiety 26, 27, 28, 29, 30 may be subjected to deep analysis of the influence on either 5-HT₆R or ADMET effects *in vitro*. The presented modification resulted in a rather significant decrease in affinity for the 5-HT₆R but these values are still below 500 nM. More importantly, N-demethylated compounds 26 and 28 remarkably reduce H₂O₂-induced oxidation in both cell lines HepG2 and SH-SY5Y in contrast to sulfur methyl derivatives 19, 22, which appeared to be inactive in this test. Concerning the HepG2 cell line, compounds 26 and 28 have been shown to be highly potent antioxidants with IC₅₀ values 0.02 ± 0.10 for the oxygen derivative (26) and 0.052 ± 0.020 for the sulfur one (28). Also noteworthy are compounds 5 and 12 (an oxygen derivatives with a N-methylpiperazine moiety), which show moderate antioxidant activity in both cell lines. Recent studies have linked neuronal death, a major cause of Alzheimer's disease, to free radicals and oxidative damage [61–65]. This is why neuroprotective molecules entering the brain are so valuable, and more effective treatments for central nervous system disorders can be implemented. Finally, the determined viability of both, SHSY-5Y and HepG2 cells in the presence of compound 22 and its demethylated metabolite 30 have shown that the toxicity of the metabolite slightly increased in comparison to the parent structure at the concentration of 50 μM .

Comparing the *in vivo* studies results for the 2,5-dichlorophenyl thioether triazine derivative 19 to the previously investigated O-ether

analogues: the direct (5) as well as the 2,3-dichlorophenyl (8) and the phenyl unsubstituted (4), a significant change against the introduction of sulfur in place of oxygen can be seen. All O-derivatives (4, 5 and 8) showed potent or very potent memory reversal effects, even at doses < 1 mg/kg [15,23] together with various anxiolytic or antidepressant-like actions, while the thioether 19 showed only antidepressant-like effects. This is apparently a consequence of a change in the mechanism of the intrinsic activity, probably not only related to agonism observed for 19, but also to the much lower agonistic potency, inadequate to the affinity observed in the radioligand binding assay. This suggests a more complicated, not only agonistic, mechanism of an intrinsic activity of 19, which is unable to identify on the basis of the performed biological studies.

3.2. BBB-permeability

The series of triazine derivatives (1–30) was designed in search for potential AD agents, i.e. CNS therapeutics. Thus, their ability to cross the blood-brain barrier (BBB) and availability for the targets engagement in the brain is a crucial property required. Due to the presence of 6 nitrogen atoms within the molecule, the ability of the triazine compounds to penetrate the blood-brain barrier may be questionable, in particular, if taking into account the criteria and rules of permeability through the BBB developed over the last 20 years. The older BBB-classification system directly (e.g. Norinder and Haeberlein rule) [66] or indirectly (equations of Zhao) [67], indicate an upper limit of N-atoms in the molecule to readily penetrate BBB. In agreement with them, the newest models of BBB/CNS-permeability estimation, indicated that non-CNS-penetrating compounds have a larger number of HBDS and HBAS [68], in which N-containing moieties can contribute significantly.

In this context, all new compounds 14–30 and previously obtained 4, 5 and 8 were subjected to simulation of the ability to cross BBB and penetrate into the CNS using bioinformatics tools pkCSM [69] and SwissADME [70]. The results obtained (see SI, Fig. S11, Table S5) were compared with *in vitro* and *in vivo* experimental data coming from both, previous and current assays performed for selected members (4, 5, 8, 19 and 22).

According to the prediction with SwissADME tool, the whole series should be poorly BBB penetrating. The program pkCSM indicated that most of the compounds (4, 8, 13–19, 22,23, 25–28 and 30) represent moderate ability to penetrate BBB, while four compounds 20, 21, 29 and 5 belong to those poorly distributed to the brain. In the case of CNS-permeability prediction, the program showed the moderate

probability to CNS-penetration for **4**, **13–26**, **28** and **30**, indicating **5**, **8**, **27** and **29** as compounds unable to penetrate CNS.

Surprisingly, results of experimental tests performed for some members of the triazine series turned out to be much more optimistic than the *in silico* ones. First at all, the worst BBB/CNS-permeability predicted compound (**5**) was confirmed on its significant procognitive and antidepressant-like actions in the behavioral tests in rats, what indisputably proved its CNS-penetration [15]. Similarly, compound **4** and, especially **8**, doubtful for CNS penetration in the simulations carried out, was highly active in NOR test demonstrating also antidepressant-like and anxiolytic-like actions in FST and EPM tests, respectively [23]. The beneficial BBB permeability of **4** and **8** was also confirmed “directly” in the pharmacokinetics studies *in vivo* in rats [23]. The antidepressant-like and procognitive, however slight, actions of **19** prove the compound to penetrate BBB/CNS, as well. Furthermore, all the compounds (**4**, **5**, **8**, **19** and **22**) were confirmed well-permeable in Caco-2 assay, and **4**, **5** and **8** – the highly permeable ones [23] in PAMPA model, which is a strongly simplified representation of the BBB looking only at transcellular diffusion [68].

Taking into account that all examined *in silico* representatives of the series displayed logBB and logPS parameters more favorable for BBB permeation than those predicted for **5** (Table S5), and the majority of them (**4**, **13–26**, **28** and **30**) exerted also better CNS-permeability parameters over **8**, it can be expected that the whole triazine series should penetrate CNS at least at the corresponding level to **5** or **8**.

4. Conclusions

The newly designed and synthesized 18-membered triazine-based series of 5-HT₆R ligands was extensively biologically characterized. The most exciting results brought exchange of oxygen into sulfur atom in linker, which led to different intrinsic activity. Thus, it is the first time when we found 5-HT₆R agonists in this original non-sulfone and non-indole chemical compound class. Noteworthy, targeting 5-HT₆R seems to be highly interesting as all the 5-HT₆R ligands which failed in AD patients were antagonists, and none of agonists has reached clinical trials yet. However, the new triazine 5-HT₆R agonist (**19**), selected here for the extended screening, showed weaker than expected procognitive effects, while retaining antidepressant activity characteristic of the triazine 5-HT₆R antagonist **5** [23] in rats. Due to the divergent potency of pharmacological action on 5-HT₆R in the radioligand binding- and functional assays, compound **19** seems to be a good tool-compound in the study on new cellular signaling pathways involving 5-HT₆R. The cholinesterase study carried out here for compounds **5** and **19** allowed to find a design guideline for the development of multitarget compounds with the 5-HT₆ (both agonist and antagonist)/AChE and/or BuChE mechanism in the group of 1,3,5-triazine derivatives, which may bring an innovative, effective approach for treatment of so complex disease as AD.

5. Experimental

5.1. Chemical synthesis

¹H NMR and ¹³C NMR spectra were recorded on FT-NMR 500 MHz spectrometer JEOL JNM-ECZR500 RS1 (ECZR version) at 500 and 126 MHz, respectively. All the ¹H NMR were obtained with use of DMSO-*d*₆ as deuterated solvent at ambient temperature using the solvent signal as an internal standard. The values of chemical shifts expressed as δ values in (ppm) and the coupling constants (*J*) in Hz. Data are reported as follows: chemical shift, multiplicity (s, singlet; br. s, broad singlet; d, doublet; t, triplet; dd, doublet of doublet, q, quintet, m, multiplet), coupling constant *J*, number of protons, protons position. Mass spectra were recorded on a UPLC-MS/MS system consisted of a Waters ACQUITY®UPLC® (Waters Corporation, Milford, MA, USA), which is coupled to a Waters TQD mass spectrometer (electrospray ionization

mode ESI-tandem quadrupole). The UPLC/MS purity of all the final compounds was confirmed to be higher than 95%. Retention time values (*t*_R) are given in minutes. HRMS spectra were recorded on the UPLC-QToF system consisted of a Waters Acquity I-Class Plus (Waters Corporation, Milford, MA, USA) coupled to a Waters Synapt XS mass spectrometer (electrospray ionization mode ESI). Chromatographic separations were carried out using the Acquity UPLC BEH (bridged ethylene hybrid) C18 column; 2.1 × 100 mm, and 1.7 μm particle size, equipped with Acquity UPLC BEH C18 VanGuard pre-column; 2.1 × 5 mm, and 1.7 μm particle size. The column was maintained at 40 °C, and eluted under gradient conditions using from 95% to 0% of eluent A over 10 min, at a flow rate of 0.3 mL min⁻¹. Eluent A: water/formic acid (0.1%, v/v); eluent B: acetonitrile/formic acid (0.1%, v/v).

Chromatograms were recorded using Waters eλ PDA detector. Spectra were analyzed in 200–700 nm range with 1.2 nm resolution and sampling rate 20 points/s.

MS detection settings of Waters Synapt XS mass spectrometer were as follows: source temperature 150 °C, desolvation temperature 350 °C, desolvation gas flow rate 600 L h⁻¹, cone gas flow 100 L h⁻¹, capillary potential 3.00 kV, cone potential 30 V. Nitrogen was used for both nebulizing and drying gas. The data were obtained in a resolution scan mode ranging from 50 to 1000 *m/z* in time 0.1 s intervals. Leu-enkephalin was used as a mass reference compound.

Data acquisition software was MassLynx V 4.2 (Waters).

Thin-layer chromatography (TLC) was performed on pre-coated Merck silica gel 60 F254 aluminum sheets. The reactions at fixed temperature were carried out using a magnetic stirrer with a contact thermometer Heidolph MR 2001. Intermediates (**32–44**) were synthesized based on previous methods [15,24], and used in a crude form for synthesis of the final compounds (**13–30**). Details of the characterizations of the new synthesis intermediates **36,38–44** are given in Supplementary Information. Aromatic ether intermediates **32,34,35,37** are commercially available reagents, however they were synthesized because of high costs (appropriate CAS numbers and PubChem compound ID are given in Supplementary Information).

5.1.1. General procedure for the synthesis of final compounds 13–25

Sodium (10 mmol, 2eq) was dissolved in 20 mL of absolute methanol, then 4-methylpiperazine-1-yl biguanide hydrochloride (5 mmol, 1eq) and a proper ester (5 mmol, 1eq) was added. The reaction mixture was refluxed for 15–30 h. Subsequently, the reaction mixture was cooled down to room temperature and water was added (~10 mL). The occurred precipitate was isolated by filtration and crystallized from methanol to give the desired final product as solid (method A). When precipitate did not appear, the product was converted into hydrochloric form using 2 M solution of HCl in diethyl ether (method B).

5.1.1.1. 4-(2-(2-chlorophenoxy)propan-2-yl)-6-(4-methylpiperazin-1-yl)-1,3,5-triazin-2-amine (13). Ester 32, reaction time: 16 h. Method B.

White solid. Yield 35%. C₁₇H₂₃ClN₆O (MW 362.86), LC/MS⁺: purity: 99%, *t*_R = 3.85, (ESI) *m/z* [M+H]⁺ found: 363.19. HRMS [ESI+]: [M+H]⁺ found: 363.178. ¹H NMR (500 MHz, DMSO-*d*₆): δ 11.89 (br. s, 1H), 8.44 (d, 2H, *J* = 185.9 Hz, NH₂), 7.26 (t, 1H, *J* = 8.1 Hz, Ar-3-H), 7.09 (d, 2H, *J* = 8.1 Hz, Ar-4,5-H), 6.90 (d, 1H, *J* = 7.7 Hz Ar-6-H), 3.51 (m, 5H, Pp-2,6-H), 3.06 (br. s, 3H, Pp-3,5-H), 2.72 (d, 3H, *J* = 3.6 Hz, N-CH₃), 1.59 (s, 6H, 2xCH₃). ¹³C NMR (126 MHz, DMSO-*d*₆) δ 178.52, 173.85, 167.57, 165.02, 164.96, 157.41, 156.49, 156.43, 133.85, 133.35, 131.25, 130.72, 122.53, 121.04, 119.40, 118.86, 117.67, 81.64, 79.73, 54.70, 52.98, 46.21, 26.88, 25.38.

5.1.1.2. 4-(2-((2-chlorophenyl)thio)propan-2-yl)-6-(4-methylpiperazin-1-yl)-1,3,5-triazin-2-amine (14). Ester 33, reaction time: 16 h. Method B.

White solid. Yield 27%. C₁₇H₂₃ClN₆S (MW 378.92), LC/MS⁺: purity: 100%, *t*_R = 4.17, (ESI) *m/z* [M+H]⁺ found: 379.17. HRMS [ESI+]: [M+H]⁺ found: 379.148. ¹H NMR (500 MHz, DMSO-*d*₆): δ 7.45 (dd, 1H,

$J = 8.0, 1.3$ Hz, Ar-3-H), 7.37 (dd, 1H, $J = 7.7, 1.7$ Hz, Ar-6-H), 7.32 (td, 1H, $J = 7.7, 1.7$ Hz, Ar-5-H), 7.21 (td, 1H, $J = 7.5, 1.4$ Hz, Ar-4-H), 6.73 (br. s, 2H, NH₂), 3.49 (d, 4H, $J = 74.5$ Hz, Pp-2,6-H), 2.18 (br. s, 4H, Pp-3,5-H), 2.13 (s, 3H, N-CH₃), 1.53 (s, 6H, 2xCH₃). ¹³C NMR (126 MHz, DMSO-*d*₆) δ 178.80, 167.60, 164.79, 139.55, 138.83, 132.13, 130.86, 130.21, 127.48, 54.86, 54.72, 54.71, 46.33, 42.82, 27.34.

5.1.1.3. (RS)-4-(1-((2,5-dichlorophenyl)thio)ethyl)-6-(4-methylpiperazin-1-yl)-1,3,5-triazin-2-amine (15). Ester **34**, reaction time: 16 h. Method A. White solid. Yield 24%. C₁₆H₂₀Cl₂N₆S (MW 399.34), LC/MS⁺: purity: 98%, $t_R = 4.62$, (ESI) m/z [M+H]⁺ found: 399.05. HRMS [ESI+]: [M+H]⁺ found: 399.092. ¹H NMR (500 MHz, DMSO-*d*₆): 7.83 (d, $J = 2.4$, Hz, 1H, Ar-6-H), 7.47 (d, $J = 8.6$ Hz, 1H, Ar-3-H), 7.25 (dd, $J = 8.6, 2.4$ Hz, 1H, Ar-4-H), 6.97 (d, 1H, NH₂), 4.30 (q, $J = 7.0$ Hz, 1H, CH), 3.75–3.62 (br. m, 4H, Pp-2,6-H), 2.29 (br. m, 4H, Pp-3,5-H), 2.19 (s, 3H, CH₃), 1.56 (d, $J = 7.0$ Hz, 3H, CH₃). ¹³C NMR (126 MHz, DMSO-*d*₆) δ 177.33, 167.58, 164.58, 138.26, 132.63, 131.28, 130.19, 127.00, 19.27.

5.1.1.4. (RS)-4-(1-((3,4-dichlorophenyl)thio)ethyl)-6-(4-methylpiperazin-1-yl)-1,3,5-triazin-2-amine (16). Ester **35**, reaction time: 16 h. Method A. White solid. Yield 35%. C₁₆H₂₀Cl₂N₆S (MW 399.34), LC/MS⁺: purity: 100%, $t_R = 4.65$, (ESI) m/z [M+H]⁺ found: 399.05. HRMS [ESI+]: [M+H]⁺ found: 399.100. ¹H NMR (500 MHz, DMSO-*d*₆): δ 7.67 (s, 1H, Ar-2-H), 7.48 (d, 1H, $J = 8.1$ Hz, Ar-5-H), 7.31 (d, 1H, $J = 7.5$ Hz, Ar-6-H), 6.87 (br. d, $J = 42.1$ Hz, NH₂), 4.15 (m, 1H, CH), 3.58 (br. s, 4H, Pp-2,6-H), 2.21 (s, 4H, Pp-3,5-H), 2.13 (s, 3H, N-CH₃), 1.46 (d, $J = 6.4$ Hz, 3H, CH₃). ¹³C NMR (126 MHz, DMSO-*d*₆) δ 177.28, 167.55, 164.65, 137.27, 131.83, 131.53, 131.08, 130.39, 129.36, 54.80, 48.31, 46.29, 19.30.

5.1.1.5. (RS)-4-(1-((3,5-dichlorophenyl)thio)ethyl)-6-(4-methylpiperazin-1-yl)-1,3,5-triazin-2-amine (17). Ester **36**, reaction time: 16 h. Method A. White solid. Yield 35%. C₁₆H₂₀Cl₂N₆S (MW 399.34), LC/MS⁺: purity: 100%, $t_R = 4.86$, (ESI) m/z [M+H]⁺ found: 399.10. HRMS [ESI+]: [M+H]⁺ found: 399.092. ¹H NMR (500 MHz, DMSO-*d*₆): δ 7.51–7.48 (m, 2H, Ar-2,6-H), 7.42–7.39 (m, 1H, Ar-4-H), 6.93 (d, $J = 38.2$ Hz, 2H, NH₂), 4.31–4.24 (m, 1H, CH), 3.66 (br. m, 4H, Pp-2,6-H), 2.27 (br. m, 4H, Pp-3,5-H), 2.17 (s, 3H, N-CH₃), 1.54–1.48 (d, $J = 7.1$ Hz, 3H, CH₃). ¹³C NMR (126 MHz, DMSO-*d*₆) δ 177.35, 167.57, 166.93, 164.64, 141.00, 134.66, 127.32, 126.02, 125.90, 47.69, 46.30, 19.27.

5.1.1.6. (RS)-4-(4-methylpiperazin-1-yl)-6-(1-(phenylthio)propyl)-1,3,5-triazin-2-amine (18). Ester **37**, reaction time: 16 h. Method B. White solid. Yield 31%. C₁₇H₂₄N₆S (MW 344.48), LC/MS⁺: purity: 100%, $t_R = 3.80$, (ESI) m/z [M+H]⁺ found: 345.21. HRMS [ESI+]: [M+H]⁺ found: 345.187. ¹H NMR (500 MHz, DMSO-*d*₆): δ 11.68 (br. s, 1H, NH⁺), 8.34–7.63 (d, 1H, NH₂), 7.43–7.37 (m, 2H, Ar-2,6-H), 7.34–7.25 (m, 3H, Ar-3,4,5-H), 4.49 (br. s, 2H, Pp-2-H), 3.99 (t, $J = 7.4$ Hz, 1H, CH), 3.38 (m, 4H, Pp-3,5-H), 2.94 (br. s, 2H, Pp-6-H), 2.70 (s, 3H, N-CH₃), 1.89 (m, 2H, CH₂), 0.93 (t, $J = 7.3$ Hz, 3H, CH₃). ¹³C NMR (126 MHz, DMSO-*d*₆) δ 171.90, 132.41, 131.87, 129.10, 127.72, 51.97, 50.84, 24.53, 11.38.

5.1.1.7. (RS)-4-(1-((2,5-dichlorophenyl)thio)propyl)-6-(4-methylpiperazin-1-yl)-1,3,5-triazin-2-amine (19). Ester **38**, reaction time: 16 h. Method A. White solid. Yield 21%. C₁₇H₂₂Cl₂N₆S (MW 413.37), LC/MS⁺: purity: 100%, $t_R = 5.12$, (ESI) m/z [M+H]⁺ found: 413.19. HRMS [ESI+]: [M+H]⁺ found: 413.111. ¹H NMR (500 MHz, DMSO-*d*₆): 7.83 (d, $J = 5.9$ Hz, 1H, Ar-6-H), 7.45 (d, $J = 8.5$ Hz, 1H, Ar-3-H), 7.24 (dd, $J = 8.5, 2.4$ Hz, 1H, Ar-4-H), 7.02–6.85 (2, 2H, NH₂), 4.04 (t, $J = 6.3$ Hz, 1H, CH), 3.84–3.54 (br. m, 4H, Pp-2,6-H), 2.38–2.21 (br. m, 4H, Pp-3,5-H), 2.18 (s, 3H, N-CH₃), 2.09–1.99 (m, 1H, CH₂), 1.91–1.82 (m, 1H, CH₂), 0.94 (t, $J = 7.3$ Hz, 3H, CH₃). ¹³C NMR (126 MHz, DMSO-*d*₆): δ 176.66, 167.60, 164.56, 138.40, 132.61, 131.26, 130.16, 128.57, 126.91, 53.53, 46.28, 26.36, 12.34.

5.1.1.8. (RS)-4-(1-((3,4-dichlorophenyl)thio)propyl)-6-(4-methylpiperazin-1-yl)-1,3,5-triazin-2-amine (20). Ester **39**, reaction time: 16 h. Method A. White solid. Yield 35%. C₁₇H₂₂Cl₂N₆S (MW 413.37), LC/MS⁺: purity: 98%, $t_R = 5.06$, (ESI) m/z [M+H]⁺ found: 413.19. HRMS [ESI+]: [M+H]⁺ found: 413.111. ¹H NMR (500 MHz, DMSO-*d*₆): δ 7.72–7.70 (m, 1H, Ar-2-H), 7.53–7.51 (m, 1H, Ar-6-H), 7.36–7.33 (m, 1H, Ar-5-H), 6.89 (d, $J = 37.1$ Hz, 2H, NH₂), 3.93 (t, $J = 7.3$ Hz, 1H, CH), 3.70–3.54 (br. s, 4H, Pp-2,6-H), 2.32–2.21 (br. s, 4H, Pp-3,5-H), 2.17 (s, 3H, N-CH₃), 2.02–1.95 (m, 1H, CH₂), 1.86–1.78 (m, 1H, CH₂), 0.91 (t, $J = 7.1$ Hz, 3H, CH₃). ¹³C NMR (126 MHz, DMSO-*d*₆) δ 176.62, 167.52, 164.62, 137.33, 131.80, 131.44, 131.09, 130.36, 129.30, 55.12, 46.27, 26.24, 12.30.

5.1.1.9. (RS)-4-(1-((3,5-dichlorophenyl)thio)propyl)-6-(4-methylpiperazin-1-yl)-1,3,5-triazin-2-amine (21). Ester **40**, reaction time: 16 h. Method A. White solid. Yield 45%. C₁₇H₂₂Cl₂N₆S (MW 413.37), LC/MS⁺: purity: 100%, $t_R = 5.38$, (ESI) m/z [M+H]⁺ found: 413.26. HRMS [ESI+]: [M+H]⁺ found: 413.111. ¹H NMR (500 MHz, DMSO-*d*₆): δ 7.49 (d, Hz, 2H, Ar-2,6-H), 7.39 (s, 1H, Ar-4-H), 6.92 (d, $J = 37.4$ Hz, 2H, NH₂), 4.03–3.98 (t, 1H, CH), 3.62 (br. s, 4H, Pp-2,6-H), 2.36–2.20 (br. m, 4H, Pp-3,5-H), 2.17 (s, 3H, N-CH₃), 2.04–1.94 (m, 1H, CH₂), 1.87–1.77 (m, 1H, CH₂), 0.91 (t, $J = 8.2$ Hz, 3H, CH₃). ¹³C NMR (126 MHz, DMSO-*d*₆) δ 176.74, 167.56, 164.61, 141.10, 134.65, 127.20, 125.83, 46.27, 26.21, 12.29.

5.1.1.10. (RS)-4-(1-((2,3-dichlorophenyl)thio)propyl)-6-(4-methylpiperazin-1-yl)-1,3,5-triazin-2-amine (22). Ester **41**, reaction time: 16 h. Method A. White solid. Yield 36%. C₁₇H₂₂Cl₂N₆S (MW 413.37), LC/MS⁺: purity: 100%, $t_R = 5.02$, (ESI) m/z [M+H]⁺ found: 413.19. HRMS [ESI+]: [M+H]⁺ found: 413.111. ¹H NMR (500 MHz, DMSO-*d*₆): δ 7.62 (d, $J = 7.9$ Hz, 1H, Ar-4-H), 7.44 (d, $J = 8.0$ Hz, 1H, Ar-6-H), 7.35–7.22 (m, 1H, Ar-5-H), 6.94 (d, $J = 46.7$ Hz, 2H, NH₂), 4.01 (t, $J = 14.8, 8.8$ Hz, 1H, CH), 3.64 (s, 4H, Pp-2,6-H), 2.26 (s, 4H, Pp-3,5-H), 2.17 (s, 3H, N-CH₃), 2.08–1.99 (m, 1H, CH₂), 1.93–1.83 (m, 1H, CH₂), 0.94 (t, $J = 9.4$ Hz, 3H, CH₃). ¹³C NMR (126 MHz, DMSO-*d*₆) δ 176.32, 167.46, 165.40, 164.73, 138.72, 132.56, 128.77, 128.36, 127.83, 100.00, 54.24, 46.29, 26.62, 12.30.

5.1.1.11. (RS)-4-(1-((2,5-dichlorophenyl)thio)butyl)-6-(4-methylpiperazin-1-yl)-1,3,5-triazin-2-amine (23). Ester **42**, reaction time: 16 h. Method A. White solid. Yield 53%. C₁₈H₂₄Cl₂N₆S (MW 427.39), LC/MS⁺: purity: 99%, $t_R = 5.36$, (ESI) m/z [M+H]⁺ found: 427.22. HRMS [ESI+]: [M+H]⁺ found: 427.122. ¹H NMR (500 MHz, DMSO-*d*₆): δ 7.77 (d, $J = 2.4$ Hz, 1H, Ar-6-H), 7.41 (d, $J = 8.5$ Hz, 1H, Ar-3-H), 7.19 (dd, $J = 8.5, 2.4$ Hz, 1H, Ar-4-H), 6.90 (d, $J = 55.8$ Hz, 2H, NH₂), 4.05 (dd, $J = 8.5, 6.6$ Hz, 1H, CH), 3.82–3.48 (br. m, 4H, Pp-2,6-H), 2.24 (br. m, 4H, Pp-3,5-H), 2.13 (s, 3H, N-CH₃), 2.01–1.90 (m, 1H, CH₂), 1.82–1.69 (m, 1H, CH₂), 1.44–1.21 (m, 2H, CH₂), 0.84 (t, $J = 7.4$ Hz, 3H, CH₃). ¹³C NMR (126 MHz, DMSO-*d*₆): δ 176.80, 167.60, 164.54, 138.39, 132.59, 131.26, 130.15, 128.55, 126.92, 51.58, 46.29, 35.09, 20.55, 14.17.

5.1.1.12. (RS)-4-(1-((3,5-dichlorophenyl)thio)butyl)-6-(4-methylpiperazin-1-yl)-1,3,5-triazin-2-amine (24). Ester **43**, reaction time: 16 h. Method A. White solid. Yield 37%. C₁₈H₂₄Cl₂N₆S (MW 427.39), LC/MS⁺: purity: 100%, $t_R = 5.81$, (ESI) m/z [M+H]⁺ found: 427.22. HRMS [ESI+]: [M+H]⁺ found: 427.130. ¹H NMR (500 MHz, DMSO-*d*₆): δ 7.48 (d, $J = 1.8$ Hz, 2H, Ar-2,6-H), 7.39 (t, $J = 1.8$ Hz, 1H, Ar-4-H), 6.92 (d, $J = 44.2$ Hz, 2H, NH₂), 4.08–4.03 (m, 1H, CH), 3.77–3.54 (br. s, 4H, Pp-2,6-H), 2.34–2.20 (br. s, 4H, Pp-3,5-H), 2.17 (s, 3H, N-CH₃), 2.01–1.92 (m, 1H, CH₂), 1.80–1.72 (m, 1H, CH₂), 1.42–1.26 (m, 2H, CH₂), 0.86 (t, $J = 7.4$ Hz, 3H, CH₃). ¹³C NMR (126 MHz, DMSO-*d*₆): δ 176.90, 167.58, 164.61, 162.62, 141.12, 134.64, 127.15, 125.84, 52.71, 46.29, 35.00, 20.52, 14.19.

5.1.1.13. (RS)-4-(1-((2,3-dichlorophenyl)thio)pentyl)-6-(4-methylpiperazin-1-yl)-1,3,5-triazin-2-amine (25). Ester **44**, reaction time: 16 h. Method A White solid. Yield 45%. $C_{19}H_{26}Cl_2N_6S$ (MW 441.42), LC/MS+/-: purity: 97%, $t_R = 5.98$, (ESI) m/z $[M+H]^+$ 441.24. HRMS [ESI+]: $[M+H]^+$ found: 441.145. 1H NMR (500 MHz, DMSO- d_6): δ 7.45 (dd, 1H, $J = 8.0$, 1.4 Hz, Ar-4-H), 7.24 (dd, $J = 8.0$, 1.4 Hz, 1H, Ar-6-H), 7.05 (t, 1H, $J = 8.0$ Hz, Ar-5-H), 5.01 (s, 2H, NH_2), 4.00 (dd, 1H, $J = 8.3$, 6.6 Hz, CH), 3.76 (br. s, 4H, Pp-2,6-H), 2.37 (br. s, 4H, Pp-3,5-H), 2.30 (s, 3H, $N-CH_3$), 2.19–1.84 (m, 2H, CH_2), 1.52–1.28 (m, 4H, CH_2-CH_2), 0.87 (t, 3H, $J = 7.2$ Hz, CH_3). ^{13}C NMR (126 MHz, DMSO- d_6): δ 176.52, 167.49, 164.73, 138.70, 132.58, 130.00, 128.76, 128.40, 127.87, 52.76, 46.29, 32.99, 29.45, 22.38, 14.31.

5.1.2. General procedure for the synthesis of final compounds 26–30

Compound (**4,5,8,19,22**) (2.5 mmol, 1 eq.) was dissolved in a round bottomed flask containing dry DCE (20 mL) and Et_3N (5 mmol, 1 mL, 2 eq.). The mixture was stirred at r.t. for 20 min before that 1-chloroethyl chloroformate (5 mmol, 0.38 mL, 2 eq.) was added to the solution. The mixture was left under argon atmosphere at reflux for 12 h. Then, the reaction mixture was quenched with 10 mL of water and extracted twice with 20 mL of EtOAc. The combined organic layers were washed with brine, dried over $MgSO_4$ and concentrated under reduced pressure giving a yellow-brown crude oil. The crude product was dissolved in MeOH (20 mL) and the solution was stirred at reflux for 12 h. Then the reaction mixture was concentrated by reduced pressure evaporation. Mixture of solvents (DCM, MeOH, EtOAc) was added to the residue and the precipitated product was isolated by filtration.

5.1.2.1. (RS)-4-(1-phenoxypropyl)-6-(piperazin-1-yl)-1,3,5-triazin-2-amine (26). White solid. Yield 17%. $C_{16}H_{22}N_6O$ (MW 314.39), LC/MS+/-: purity: 100%, $t_R = 3.37$, (ESI) m/z $[M+H]^+$ 315.31. HRMS [ESI+]: $[M+H]^+$ found: 315.205. 1H NMR (500 MHz, DMSO- d_6): δ 9.71 (s, 2H, $Pp-NH_2^+$), 7.22 (t, 2H, $J = 7.9$ Hz, Ar-3,5-H), 6.96–6.87 (m, 3H, Ar-2,4,6-H), 4.86 (s, 1H, CH), 3.94 (br. s, 4H, Pp-2,6-H), 3.09 (br. s, 4H, Pp-3,5-H), 1.91 (m, 2H, CH_2), 0.95 (t, 3H, $J = 7.4$ Hz, CH_3). ^{13}C NMR (126 MHz, DMSO- d_6): δ 163.13, 157.99, 130.03, 121.85, 116.17, 79.44, 42.55, 27.42, 9.97.

5.1.2.2. (RS)-4-(1-(2,5-dichlorophenoxy)propyl)-6-(piperazin-1-yl)-1,3,5-triazin-2-amine (27). White solid. Yield 70%. $C_{16}H_{20}Cl_2N_6O$ (MW 383.28), LC/MS+/-: purity: 99%, $t_R = 4.49$, (ESI) m/z $[M+H]^+$ 383.22. HRMS [ESI+]: $[M+H]^+$ found: 383.116. 1H NMR (500 MHz, DMSO- d_6): δ 9.59 (s, 2H, $Pp-NH_2^+$), 7.44 (d, 1H, $J = 8.5$ Hz, Ar-3-H), 7.13 (d, 1H, $J = 2.3$ Hz, Ar-6-H), 6.99 (dd, 1H, $J = 8.5$, 2.3 Hz, Ar-4-H), 5.04 (t, 1H, $J = 6.1$ Hz, CH), 3.91 (br. s, 4H, Pp-2,6-H), 3.11 (br. s, 4H, Pp-3,5-H), 2.04–1.93 (m, 2H, CH_2), 0.97 (t, 3H, $J = 7.4$ Hz, CH_3). ^{13}C NMR (126 MHz, DMSO- d_6): δ 162.93, 154.48, 132.66, 131.62, 122.77, 121.63, 116.54, 80.70, 80.70, 27.24, 27.24, 11.46, 11.46, 9.82, 9.82.

5.1.2.3. (RS)-4-(1-((2,5-dichlorophenyl)thio)propyl)-6-(piperazin-1-yl)-1,3,5-triazin-2-amine (28). White solid. Yield 25%. $C_{16}H_{20}Cl_2N_6S$ (MW 399.34), LC/MS+/-: purity: 99%, $t_R = 4.69$, (ESI) m/z $[M+H]^+$ 399.17. HRMS [ESI+]: $[M+H]^+$ found: 399.092. 1H NMR (500 MHz, DMSO- d_6): δ 9.65 (s, 2H, $Pp-NH_2^+$), 7.76 (d, 1H, $J = 2.4$ Hz, Ar-6-H), 7.47 (d, 1H, $J = 8.5$ Hz, Ar-3-H), 7.28 (dd, 1H, $J = 8.5$, 2.4 Hz, Ar-4-H), 4.22 (t, 1H, $J = 7.4$ Hz, CH), 3.9 (br. s, 4H, Pp-2,6-H), 3.11 (br. s, 4H, Pp-3,5-H), 2.06 (dq, 1H, $J = 15.0$, 7.4 Hz, CH_2), 1.92 (dq, 1H, $J = 14.0$, 6.9 Hz, CH_2), 0.95 (t, 3H, $J = 7.3$ Hz, CH_3). ^{13}C NMR (126 MHz, DMSO- d_6): δ 162.39, 136.04, 132.70, 131.72, 131.52, 130.36, 128.30, 51.43, 25.45, 12.07, 11.46.

5.1.2.4. (RS)-4-(1-(2,3-dichlorophenoxy)propyl)-6-(piperazin-1-yl)-1,3,5-triazin-2-amine (29). White solid. Yield 15%. $C_{16}H_{20}Cl_2N_6O$ (MW 383.28), LC/MS+/-: purity: 98%, $t_R = 4.54$, (ESI) m/z $[M+H]^+$ 383.22. HRMS [ESI+]: $[M+H]^+$ found: 383.116. 1H NMR (500 MHz, DMSO- d_6):

δ 9.46 (s, 1H, $Pp-NH_2^+$), 7.18 (t, 1H, $J = 8.2$ Hz, Ar-5-H), 7.13 (dd, 1H, $J = 8.1$, 1.3 Hz, Ar-4-H), 6.86 (dd, 1H, $J = 8.3$, 1.2 Hz, Ar-6-H), 4.80 (t, 1H, $J = 6.3$ Hz, CH_2), 3.84 (br. s, 1H, Pp-2,6-H), 3.05 (br. s, 4H, Pp-3,5-H), 1.94 (p, 2H, $J = 7.2$ Hz, CH_2), 0.99 (t, 3H, $J = 7.4$ Hz, CH_3). ^{13}C NMR (126 MHz, DMSO- d_6): δ 164.74, 155.78, 132.82, 128.85, 122.57, 120.94, 113.88, 82.34, 27.89, 10.34.

5.1.2.5. (RS)-4-(1-((2,3-dichlorophenyl)thio)propyl)-6-(piperazin-1-yl)-1,3,5-triazin-2-amine (30). White solid. Yield 2%. $C_{16}H_{20}Cl_2N_6S$ (MW 399.34), LC/MS+/-: purity: 100%, $t_R = 4.88$, (ESI) m/z $[M+H]^+$ 399.17. HRMS [ESI+]: $[M+H]^+$ found: 399.092. 1H NMR (500 MHz, DMSO- d_6): δ 9.31 (s, 2H, $Pp-NH_2^+$), 7.59 (d, $J = 7.9$ Hz, 1H, Ar-4-H), 7.45 (d, $J = 7.9$ Hz, 1H, Ar-6-H), 7.30 (t, 7.9 Hz, 1H Ar-5-H), 4.14–4.02 (m, 1H, CH), 3.87 (br. s, Pp-2,6-H), 3.08 (br. s, Pp-3,5-H), 2.12–1.79 (m, 2H, CH_2), 0.92 (t, $J = 7.3$ Hz, 3H, CH_3). ^{13}C NMR (126 MHz, DMSO- d_6): δ 176.34, 167.45, 164.74, 138.77, 132.57, 129.84, 128.79, 128.25, 127.78, 54.22, 26.65, 12.30.

5.2. X-ray crystallographic studies

Crystals suitable for an X-ray structure analysis were obtained from propan-1-ol for **19** and from propan-2-ol for **1** by slow evaporation of the solvent at room temperature.

Data for single crystals were collected using the XtaLAB Synergy-S diffractometer, equipped with the Cu (1.54184 Å) $K\alpha$ radiation source and graphite monochromator. The phase problem was solved by direct methods using SHELXTL [71] for **19** and SIR-2014 [72] for **1**. All non-hydrogen atoms were refined anisotropically using weighted full-matrix least-squares on F^2 . Refinement and further calculations were carried out using SHELXL [73]. The hydrogen atoms bonded to carbons were included in the structure at idealized positions and were refined using a riding model with $U_{iso}(H)$ fixed at 1.5 $U_{eq}(C)$ for methyl groups and 1.2 $U_{eq}(C)$ for the other hydrogen atoms. Hydrogen atoms attached to nitrogen atoms were found from the difference Fourier map and refined without any restraints. Compound **19** crystallizes together with propan-1-ol molecule which is disordered. The occupancy factors after refinement for this molecule are 0.52(1) and 0.48(1) for the major and minor components, respectively. For molecular graphics MERCURY [4] program was used.

5.2.1. Crystallographic data

19: $C_{17}H_{22}Cl_2N_6S \cdot C_3H_8O$, $M_r = 473.46$, wavelength 1.54184 Å, crystal size = $0.08 \times 0.20 \times 0.41$ mm³, triclinic, space group $P\bar{1}$ $a = 9.7591(3)$ Å, $b = 11.5433(4)$ Å, $c = 11.9877(4)$ Å, $\alpha = 72.603(3)^\circ$, $\beta = 72.131(2)^\circ$, $\gamma = 72.484(2)^\circ$, $V = 1193.51(7)$ Å³, $Z = 2$, $T = 100(2)$ K, 32510 reflections collected, 5002 unique reflections ($R_{int} = 0.0694$), $R1 = 0.0653$, $wR2 = 0.1842$ [$I > 2\sigma(I)$], $R1 = 0.0700$, $wR2 = 0.1891$ [all data].

1: $C_{16}H_{20}Cl_2N_6O$, $M_r = 383.28$, wavelength 1.54184 Å, crystal size = $0.05 \times 0.20 \times 0.24$ mm³, monoclinic, space group $P2_1/c$, $a = 10.2893(1)$ Å, $b = 9.2131(1)$ Å, $c = 19.1785(3)$ Å, $\beta = 102.367(1)^\circ$, $V = 1775.87(3)$ Å³, $Z = 4$, $T = 100(2)$ K, 51628 reflections collected, 3694 unique reflections ($R_{int} = 0.0549$), $R1 = 0.0486$, $wR2 = 0.1247$ [$I > 2\sigma(I)$], $R1 = 0.0500$, $wR2 = 0.1257$ [all data].

CCDC 2269009–2269010 contain the supplementary crystallographic data. These data can be obtained free of charge from The Cambridge Crystallographic Data Centre via www.ccdc.cam.ac.uk/data_request/cif.

5.3. Evaluation of 5-HT₆R, 5-HT_{2A}R, 5-HT₇R, D₂R affinities

5.3.1. Cell culture and preparation of cell membranes for radioligand binding assays

HEK293 cells with stable expression of human 5-HT₆, 5-HT_{7b} and D₂L receptors (prepared with the use of Lipofectamine 2000) or CHOeK1

cells with plasmid containing the sequence coding for the human serotonin 5-HT_{2A} receptor (PerkinElmer) were maintained at 37 °C in a humidified atmosphere with 5% CO₂ and grown in Dulbecco's Modified Eagle Medium containing 10% dialyzed fetal bovine serum and 500 mg/mL G418 sulfate. For membrane preparation, cells were subcultured in 150 cm² flasks, grown to 90% confluence, washed twice with prewarmed to 37 °C phosphate buffered saline (PBS) and pelleted by centrifugation (200×g) in PBS containing 0.1 mM EDTA and 1 mM dithiothreitol. Prior to membrane preparation, pellets were stored at –80 °C.

5.3.2. Radioligand binding assays

Cell pellets were thawed and homogenized in 10 vol of assay buffer using an Ultra Turrax tissue homogenizer and centrifuged twice at 35,000 g for 15 min at 4 °C, with incubation for 15 min at 37 °C in between. The composition of the assay buffers was as follows: for 5-HT_{2A}R: 50 mM Tris HCl, 0.1 mM EDTA, 4 mM MgCl₂ and 0.1% ascorbate; for 5-HT₆R: 50 mM Tris HCl, 0.5 mM EDTA and 4 mM MgCl₂, for 5-HT_{7B}R: 50 mM Tris HCl, 4 mM MgCl₂, 10 mM pargyline and 0.1% ascorbate; for dopamine D₂LR: 50 mM Tris HCl, 1 mM EDTA, 4 mM MgCl₂, 120 mM NaCl, 5 mM KCl, 1.5 mM CaCl₂ and 0.1% ascorbate. All assays were incubated in a total volume of 200 μL in 96-well microtitre plates for 1 h at 37 °C, except 5-HT_{2A}R which were incubated at 27 °C. The process of equilibration was terminated by rapid filtration through Unifilter plates with a 96-well cell harvester and radioactivity retained on the filters was quantified on a Microbeta plate reader (PerkinElmer, USA). For displacement studies the assay samples contained as radioligands (PerkinElmer, USA): 1 nM [³H]-ketanserin (53.4 Ci/mmol) for 5-HT_{2A}R; 2 nM [³H]-LSD (83.6 Ci/mmol) for 5-HT₆R; 0.8 nM [³H]-5-CT (39.2 Ci/mmol) for 5-HT_{7B}R or 2.5 nM [³H]-raclopride (76.0 Ci/mmol) for D₂LR. Non-specific binding was defined with 10 mM of 5-HT in 5-HT_{7B}R binding experiments, whereas 20 mM of mianserin, 10 mM of methiothepine or 10 mM of haloperidol were used in 5-HT_{2A}R, 5-HT₆R and D₂LR assays, respectively. Each compound was tested in triplicate at 7 concentrations (10⁻¹⁰-10⁻⁴ M). The inhibition constants (K_i) were calculated from the Cheng-Prusoff equation [74]. Results were expressed as means of at least two separate experiments.

5.4. Functional assays for 5-HT₆ receptor

Test compounds were dissolved in dimethyl sulfoxide (DMSO) at a concentration of 10 mM. Serial dilutions were prepared in 96-well microplate in assay buffer and 8 concentrations were tested. For the 5-HT₆, adenylyl cyclase activity were monitored using cryopreserved 1321N1 cells with expression of the human serotonin 5-HT₆ receptor (PerkinElmer, USA). Thawed cells were resuspended in stimulation buffer (HBSS, 5 mM HEPES, 0.5 IBMX, and 0.1% BSA at pH 7.4) at 3 × 10⁵ cells/ml. The same volume (10 μL) of cell suspension was added to tested compounds. Samples were loaded onto a white opaque half area 96-well microplate. The antagonist response experiment was performed with 12 nM serotonin as the reference agonist for 5-HT₆ receptor. The agonist and antagonist were added simultaneously. Cell stimulation was performed for 30 min at room temperature. After incubation, cAMP measurements were performed with homogeneous TR-FRET immunoassay using the LANCE Ultra cAMP kit (PerkinElmer, USA). 10 μL of EucAMP Tracer Working Solution and 10 μL of ULight-anti-cAMP Tracer Working Solution were added, mixed, and incubated for 1 h. The TR-FRET signal was read on an EnVision microplate reader (PerkinElmer, USA). IC₅₀ and EC₅₀ were determined by nonlinear regression analysis using GraphPad Prism 7.0 software.

5.5. Cholinesterase inhibition assay

The test compounds for their inhibitory activity toward electric eel AChE, and horse serum BChE were evaluated by applying Ellman's assay with some modifications [39,40]. The anti-AChE activity was

determined in a reaction mixture containing 20 μL of a solution of AChE (0.9 U/mL in 0.1 M pH 8.0 phosphate buffer, PB), 20 μL of a solution of 5,5-dithio-bis-(2-nitrobenzoic) acid (DTNB 3.3 mM in 0.1 M pH 7.0 PB, containing 0.1 mM NaHCO₃), 20 μL of a solution of the test compound. In the first assay it was applied at the final concentration of 10 μM, and 120 μL of pH 8.0 PB. After incubation for 20 min at 25 °C, acetylthiocholine iodide (20 μL of 0.05 mM water solution) was added as the substrate; the hydrolysis rates of the substrate were monitored at 412 nm for 5.0 min at 25 °C, and the initial reaction rate was determined within 60 s. In determination of IC₅₀ (concentration of the inhibitor required, diminished by 50% of the rate of the control) values, five to seven concentrations of inhibitor ranging from 1 × 10⁻⁴ to 1 × 10⁻⁸ M in 0.1 M pH 8.0 PB were applied. The IC₅₀ was calculated in triplicate by nonlinear (sigmoid) regression of the response/concentration (log) curve, using Prisma GraphPad software (v. 5.01). The BChE inhibitory activity was determined similarly, by using a solution of BChE (1.8 U/mL in 0.1 M pH 8.0 PB) and butyrylthiocholine iodide (0.05 mM) as the substrate.

5.6. Molecular modelling

5.6.1. Molecular modelling to 5-HT₆R

5.6.1.1. Structures of the receptors. The structure of 5-HT₆R in the complex with agonist serotonin (PDB ID: 7XTB) [75] was retrieved from the Protein Data Bank [76].

5.6.1.2. Induced fit docking. To tune the conformation of the receptor to the studied compounds, the induced fit docking (IFD) approach from the Schrödinger package was used. Before the IFD procedure, the structure of the 5-HT₆R was prepared by assigning the bond orders, appropriate amino acid ionization states and checking for steric clashes using Protein Preparation Wizard from Schrödinger Suite. The three-dimensional structures of the ligands were prepared by LigPrep v3.6, and Epik v3.4 was used to predict the appropriate ionization states at pH = 7.4 ± 1.0.

The grid box with a size of 10 Å was centered on the co-crystallized ligand and extended searching was performed. The L-R complexes selected in the IFD procedure were next used in molecular dynamics simulations.

5.6.1.3. Molecular dynamics. A 100 ns-long molecular dynamics (MD) simulations were performed using Schrödinger Desmond software [77]. Each ligand–receptor complex was immersed into a POPC (309.5 K) membrane bilayer, which position was calculated using the PPM web server (accessed March 2, 2023). The system was solvated by water molecules described by the TIP4P potential and the OPLS3 force field was used for all atoms. 0.15 M NaCl was added to mimic the ionic strength inside the cell. The output trajectories [78] were hierarchically clustered into 5 groups according to the ligand using the trajectory analysis tool from Schrödinger Suite.

5.6.1.4. Monitoring changes in receptor conformation. To monitor changes occurring in individual fragments of the 5-HT₆R helices during molecular dynamics of a receptor between agonist and antagonist pair (5 vs. 19, and 27 vs. 28), the spatial coordinates (x,y,z) of atoms belonging to particular amino acids were converted into single points corresponding to their geometric center (i.e., centroid). This approximation allows one to track amino acid position changes by considering the trajectory of one point. The differences between receptor conformations were determined by calculating the Euclidean distance between centroids of the same amino acids (labeled as a Δd).

5.6.1.5. Quantum chemical calculations. To recognize intramolecular interactions within the studied 1,3,5-triazine derivatives, the NCIPLOT program was used [79]. First, the density functional theory (DFT)

calculations for ligand conformations determined from the MD trajectory (the most populated cluster) with the GAUSSIAN16 package [80] at the B3LYP-D3/cc-pVDZ level [81–85] with the PCM (water) [86,87] were performed. The geometry optimization of isolated ligands was performed at B3LYP-D3/cc-pVDZ level with the PCM (water). Wave functions were obtained and further used to generate reduced electron density gradient (RDG) surfaces using the NCIPLOT program. The NCI (non-covalent interaction) analysis is based on the reduced RDG defined as

$$s(r) = \frac{|\nabla\rho(r)|}{2(\pi)^{1/2}\rho(r)^{4/3}}$$

where $\nabla\rho(r)$ corresponds to a gradient of the electron density. The NCI allows visualization of both attractive and repulsive interaction regions.

5.6.2. Molecular modelling to cholinesterases

The SMILES string of ligands in both the (R) and (S) configuration was converted to three-dimensional structure within Maestro software package [88]. The proper ionization was then assigned with *fixpka* complement of QUACPAC [89], and thereafter the molecular skeleton was relaxed performing 10000 steps of Steepest Descent minimization with Open Babel [90] using the Universal Force Field while the *mol-charge* complement of QUACPAC was used to achieve Marsili-Gasteiger charges. Dockings were carried out on selected targets namely the AChE/donepezil [91] and BChE/TKN enzyme-inhibitor complexes (entry 6O4W and 7BGC in the Protein Brookhaven Database [92]). The X-ray structures were prepared with the Protein Preparation Wizard interface of Maestro removing the co-crystallized ligand and water molecules, completing the whole structure with hydrogen atoms, then optimizing their position, and assigning the ionization states of acid and basic residues according to PROPKA prediction at pH 7.0. Electrostatic charges for proteins atoms were loaded according to AMBER UNITED force field [93]. A 0.375 Å spaced boxes 60 Å × 110 Å × 50 Å for AChE and BChE, having the barycentre on the co-crystallized inhibitors poses, were considered on affinity maps calculations, and the binding site available space was screened throughout 1000 runs of Lamarckian Genetic Algorithm (LGA) implemented in AUTODOCK 4.2.6 [94] using the GPU-OpenCL algorithm version [95]. Water molecules contribution in the binding was achieved with the hydration force field parameters [96], and the population size and the number of energy evaluation figures were set to 300 and 10000000, respectively. Docking poses were ranked by ESP, a simple energy-, similarity- and population-based rule, proved to be efficient in similar structure-based studies focused on esterases ligands [97]. In this metric E accounts for the free energy of binding, the energy difference between the selected pose and the relative global minimum and the ligand efficacy, S the similarity as scored by the Tanimoto_Comb coefficient according to the shape matching algorithm ROCS [98], P is the cluster member population. The rule was applied as a cut-off threshold, judging valuable a pose only if endows a lone violation of the same rule parameters as following: FEB < -9.00, ΔE < 1.00, EFF < -0.300, TAN > 0.650, POP > 10/1000.

5.7. Drug-likeness in-vitro

5.7.1. References

The following references used in ADME-Tox studies *in vitro*: caffeine (CFN), carbonyl cyanide 3-chlorophenylhydrazone, Verapamil and doxorubicin (DX) were provided by Sigma-Aldrich (St. Louis, MO, USA).

5.7.2. Metabolic stability

The *in vitro* evaluation of metabolic pathways was performed by 120 min incubation of compounds with rat liver microsomes (RLMs) at 37 °C according the described previously procedures [99–102]. RLMs were provided by (Sigma-Aldrich, St. Louis, MO, USA). The LC/MS analyses were performed to determine the most probable structures of 5-HT₆R

ligands' metabolites.

5.7.3. Permeability Caco-2

Caco-2 cells (ATCC® no. HTB37™) were cultured in the Dulbecco's modified Eagle's Medium (DMEM, Lonza) supplemented with 20% heat-inactivated fetal bovine serum (FBS; Gibco, The-moFisher Scientific) and 1% nonessential amino acid solution (NEAA, Gibco). For the permeability study, Caco-2 cells from passage numbers 16–22 were used. Cells were seeded in Transwell inserts (polycarbonate membrane, 6.5 mm diameter and 0.4-μm pore size, Corning Costar Co., New York, USA) in 24-well plates at a density of 2 × 10⁴ cells/insert (0.33 cm²/insert) in DMEM supplemented with 20% heat-inactivated FBS, 1% NEAA, 100 U ml⁻¹ penicillin and 100 μgml⁻¹ streptomycin. The basolateral and apical compartments contained 0.1 and 0.6 mL of indicated culture medium, respectively. Before seeding the cells, the transwell inserts were prewet with a complete growth medium for 15 min. One insert (without cells) was intended as blank in the TEER (transepithelial electrical resistance) measurement. The medium was changed first after 3 h after seeding and then after 24 h to avoid multilayer formation. The culture medium was replaced every 2 days until the end of the cultivation period on day 21. On day 7 of cultivation, the medium in the apical compartments was changed to serum-free medium, whereas the basolateral medium remained the same. The transport experiment on day 21 was carried out as previously described [23]. Briefly, the inserts were carefully washed with pH 7.4. HBSS. Cell monolayer integrity was measured using the Millicell ER-2 (Millipore, Billerica, MA, USA). Inserts with a TEER value of ≥250 Ω*cm² were taken for the experiment. The transport experiment was performed in either the apical direction to the basolateral direction (A- > B, for passively transported compounds) or the basolateral direction to the apical direction (B- > A, for actively transported compounds). The tested compounds were diluted in HBSS at 10 μM and applied to the apical chamber (for A- > B) or the basolateral chamber (for B- > A), and HBSS was added to the other side. Caffeine was used as a highly permeable reference. The Caco-2 plate was then incubated for 2 h at 37 °C with a gentle shaking (150 rpm). The samples were taken from both apical and basolateral compartments, and compounds concentration was quantified by peak area analysis on the LC-MS system with internal standard (IS). The test permeability and efflux ratio for each compound were performed in triplicate. To ensure monolayer integrity throughout the experimental period, lucifer yellow (LY) rejection was measured with the EnSpire multiplate reader (PerkinElmer, Waltham, MA, USA). The *P_{app}* was calculated according to the following formula [103]:

$$P_{app} = dc/dt * V/(A * C_0)$$

dc/dt—the change in concentration in the receiving compartment overtime.

V—volume of the solution in the receiving compartment (mL).

A—surface area of the membrane (cm²).

C₀—the initial concentration in the donor compartment (μM).

Based on *in vitro/in vivo* correlation studies, the *P_{app}* values obtained from the Caco-2 assay predict the following range of *in vivo* absorption: low permeability *P_{app}* < 5 × 10⁻⁶ cm/s, high permeability *P_{app}* > 5 × 10⁻⁶ cm/s [104].

5.7.4. Hepatotoxicity and neurotoxicity

Hepatoma HepG2 (ATCC® no. HB-8065™) and the human neuroblastoma cell line SH-SY5Y (ATCC® no. CRL-2266™) were used for hepatotoxicity and neurotoxicity assessment, respectively. All assays and growth conditions were applied as we described before [99,102,105,106]. Tested compounds were added to the cells at 0.1, 1, 10, 50 and 100 μM concentration and incubated next for 72 h. The cytostatic drug doxorubicin (DX) was also added at 1 μM and used as a reference. The cells' viability was determined by CellTiter 96® AQueous Non-Radioactive Cell Proliferation Assay (MTS) provided by Promega

(Madison, WI, USA). The absorbance was measured using a microplate reader EnSpire (PerkinElmer, Waltham, MA USA) at 490 nm.

5.7.5. Antioxidant activity

5.7.5.1. Cell cultures. Human hepatocellular liver carcinoma (HepG2) cell line and human neuroblastoma cell line (SH-SY5Y) were purchased from the American Type Culture Collection (ATCC, Manassas, VA, USA) and maintained at 37 °C in a humidified atmosphere (95% air and 5% CO₂), and they were periodically screened for contamination. HepG2 cells were cultured in Eagle's Minimum Essential Medium (MEM, Euroclone S.p.A., Pero, MI, Italy), supplemented with 10% Fetal Bovine Serum (FBS, Euroclone S.p.A., Pero, MI, Italy), 1% L-glutamine (Euroclone S.p.A., Pero, MI, Italy), 100 U/mL penicillin/streptomycin (Euroclone S.p.A., Pero, MI, Italy), 1% Non-Essential Amino Acids (NEAA, Euroclone S.p.A., Pero, MI, Italy). SH-SY5Y cells were grown in a 1:1 mixture of Dulbecco's modified Eagle's medium (DMEM)—high glucose (Euroclone S.p.A., Pero, MI, Italy) and Ham's F12 Medium (Euroclone S.p.A., Pero, MI, Italy) supplemented with 10% FBS, 1% L-glutamine and 100 U/mL penicillin/streptomycin. For cell assays, cells were trypsinized using Trypsin-EDTA 1× in PBS (Euroclone S.p.A., Pero, MI, Italy).

5.7.5.2. Dichlorofluorescein assay. Generation of ROS was monitored using an oxidation-sensitive fluorescent probe, 2',7'-dichlorodihydrofluorescein diacetate (DCFH-DA, D6665; Sigma-Aldrich, St. Louis, MO) by slightly modifying the procedure reported by Wang and James [107]. Briefly, viable cells were seeded in a black 96-well cell culture plate (Costar, SigmaAldrich, St. Louis, MO, USA) and after 24 h were incubated with different concentrations (0.001–100 μM) of each compound for 1 h at 37 °C in 5% CO₂. DCFH-DA in medium without serum was added directly to each well at a final concentration of 25 μM, and the plate was incubated at 37 °C for 30 min in 5% CO₂. After washing using PBS, 100 μM H₂O₂ in medium without serum was added to each well and the cells were incubated for an additional 30 min. The formation of fluorescent dichlorofluorescein (DCF), due to oxidation of DCFH in the presence of ROS, was read at 530 nm using a microplate reader Tecan Infinite M1000 Pro (Tecan, Cernusco S.N., Italy) and DMSO medium was used for control cells. The IC₅₀ values were calculated using GraphPad Prism 9.0 (GraphPad Software, La Jolla, CA, USA). The results are expressed as mean ± SEM of at least three independent measurements in triplicate.

5.7.6. Anticoagulant action

5.7.6.1. In vitro aggregation test. *In vitro* aggregation studies were performed using freshly collected whole rat blood with a Multiplate platelet function analyzer (Roche Diagnostic, Mannheim, Germany) based on the measurements of electric impedance, according to previous procedures [47]. Blood was drawn from rats' carotid arteries with hirudin blood tube (Roche Diagnostic, Mannheim, Germany). 300 μL of hirudin anticoagulated blood was mixed with 300 μL of the prewarmed isotonic saline solution containing studied compound or vehicle (DMSO) and preincubated for 3 min at 37 °C with continuous stirring. Aspirin (Toocris, Abingdon, UK) was used as a reference compound. Aggregation was triggered by adding collagen (Hyphen-Biomed, France) at the final concentration of 1.6 μg/mL. Aggregation process was recorded for 6 min. The Multiplate software analyzed the area under the curve (AUC) of the clotting process. Each concentration of studied compounds was tested at least three times.

The results are expressed as mean ± standard deviation (SD). Statistically significant differences between groups were calculated using one-way analysis of variance (ANOVA) and the post-hoc Dunnett's test. The criterion for significance was set at $p < 0.05$.

5.8. In vivo studies

5.8.1. Animals

Eight-week-old male Wistar rats were obtained from an accredited animal facility at the Jagiellonian University Medical College, Poland. A total of 144 rats weighing 200–260 g were housed in group of four in controlled environment (ambient temperature 21 ± 2 °C; relative humidity 50–60%; 12-h light/dark cycles (lights on at 8:00)). Standard laboratory food (LSM-B) and filtered water were freely available. One week before experiments animals were handled to acclimatize to researchers' touch to minimize stress reaction of animals. Animals were assigned randomly to treatment groups. All the experiments were performed by two observers unaware of the treatment applied between 9:00 and 14:00 on separate groups of animals. All animals were used only once. All compounds were injected intraperitoneally (*i.p.*) in a volume of 2 mL/kg. Procedures involving animals and their care were conducted under current European Community and Polish legislation on animal experimentation. Additionally, all efforts were made to minimize animal suffering and to use only the number of animals necessary to produce reliable scientific data. Approval from the procedures described in this paper was obtained from the I Local Ethics Commission in Cracow (no 309/2019, July 17, 2019), complied with the European Communities Council Directive of November 24, 1986 (86/609/EEC) and were under the 1996 NIH Guide for the Care and Use of Laboratory Animals.

5.8.2. Drugs

The investigated compound 19 was suspended in 1% Tween 80 immediately before administration, while MK-801 (MK-801 maleate, Bio-Techne, Warszawa, PL) was dissolved in distilled water. All compounds were given in a volume of 2 mL/kg. Compound 19 were administered intraperitoneally (*i.p.*) 60 min while MK-801 was given *i.p.* 30 min before testing. Control animals received vehicle (1% Tween 80 (Sigma Aldrich, Poznań, PL)) according to the same schedule.

5.8.3. Behavioral procedures in rats

5.8.3.1. Novel Object Recognition (NOR) test. The protocol was adapted from the original work [108,109] and the test and the administration of compounds was done according to the previously described protocol (compound 19 and MK-801 were administered, 60 and 30 min, respectively, before T1 phase (the familiarization phase)) [23]. The discrimination index (DI) was calculated according to the formula:

$$DI = \frac{(EB - EA)}{(EA + EB)}$$

EB – the exploration time of novel object during T2 session.

EA – the exploration time of familiar object during T2 session.

MK-801 was chose as the memory disturbance-induced compound based on the literature data which indicate that selective 5-HT₆R antagonists may prevent memory disturbances in rats induced by MK-801 [23,49]. To assess the impact of the injected compounds on the rats' exploratory activity the total exploration time in T2 phase was measured.

5.8.3.2. Forced swim test (FST). The experiment was carried out according to the method of Porsolt [110] the procedure and administration of compounds was done according to the previously described protocol [23]. The immobility was assigned when no additional activity was observed other than that necessary to keep the rat's head above the water. Fresh water was used for each animal.

5.8.3.3. Elevated plus-maze test (EPM test). The testing procedure was based on a method described by Pellow and File [111]. Plus-maze apparatus (an automated device produced by Campden Instruments Ltd. (United Kingdom) made of durable, high density, non-porous black

plastic, elevated to a height of 50 cm, consisted of two open arms (50 × 10 cm) and two closed arms (50 × 10 cm, and 30 cm high walls), arranged so that the two arms of each type were opposite each other. Floor of the plus-maze was made of infrared transparent material what means that there are no visible sensors. Plus-maze apparatus was connected to PC software by control chassis. The experiments were conducted in a darkened room, only the center of the maze was illuminated with low-intensity light (30 lux measured on the maze level). Each rat was gently placed in the center of the plus-maze, facing one of the closed arms, immediately after a 5-min adaptation period in a plastic black box (60 × 60 × 35 cm), to increase the overall activity in the EPM. During a 5-min test period, automated Motor Monitor System recorded the number of entries into the closed and open arms and the time spent in either type of the arms. The device counted an effective arm-entry when the four paws of a rat were into any arm. The maze was thoroughly cleaned after each trial. EPM test is an “unconditional” anxiety-like test based on rodents’ natural aversion to heights and open space.

5.8.3.4. Exploratory activity measured in the EPM test. The experiment was performed using EPM apparatus (details see above). Total ambulation (the total distance covered by a rat, and ambulation along X and Y axis) was taken to discern drug effects on general activity from those on open-arm exploration, during a 5-min test period (i.e. the time equal to the observation period in the EPM test). Rats’ behavior was not videotaped during the test.

5.8.3.5. Statistical analysis of behavioral studies. For the statistical analysis of results STATISTICA 13 (StatSoft) was used. All behavioral results are shown as the means ± SEM. The data were evaluated by an analysis of variance (one-way ANOVA), followed by Bonferroni’s multiple comparison test; $p < 0.05$ was considered significant.

Declaration of competing interest

The authors declare that they have no known competing financial interests or personal relationships that could have appeared to influence the work reported in this paper.

Data availability

Data will be made available on request.

Acknowledgements

This study was financed by National Science Centre, Poland grant no. 2018/31/B/NZ7/O2160 and Jagiellonian University project for own research N42/DBS/000287.

Appendix A. Supplementary data

Supplementary data to this article can be found online at <https://doi.org/10.1016/j.ejmech.2023.115695>.

References

- [1] H. Ashrafian, E.H. Zadeh, R.H. Khan, Review on Alzheimer’s disease: inhibition of amyloid beta and tau tangle formation, *Int. J. Biol. Macromol.* 167 (2021) 382–394, <https://doi.org/10.1016/j.ijbiomac.2020.11.192>.
- [2] A. Sanabria-Castro, I. Alvarado-Echeverría, C. Monge-Bonilla, Molecular pathogenesis of alzheimer’s disease: an update, *Ann. Neurosci.* 24 (2017) 46–54, <https://doi.org/10.1159/000464422>.
- [3] T. Makis, M. Robert I, D. Claire S, S.-J. Tara L, *Synaptic degeneration in Alzheimer disease*, *Nat. Rev. Neurol.* 19 (2022) 19–38.
- [4] Y. Tang, D. Zhang, X. Gong, J. Zheng, A mechanistic survey of Alzheimer’s disease, *Biophys. Chem.* 281 (2022), 106735, <https://doi.org/10.1016/j.bpc.2021.106735>.
- [5] K. Sharma, Cholinesterase inhibitors as Alzheimer’s therapeutics (Review), *Mol. Med. Rep.* 20 (2019) 1479–1487, <https://doi.org/10.3892/mmr.2019.10374>.
- [6] L. Tan, Efficacy and safety of donepezil, galantamine, rivastigmine, and memantine for the treatment of Alzheimer’s disease: a systematic review and meta-analysis, *J Alzheimers Dis* 41 (2014) 615–631, <https://doi.org/10.3233/JAD-132690>.
- [7] G. Marucci, M. Buccioni, D.D. Ben, C. Lambertucci, R. Volpini, F. Amenta, Efficacy of acetylcholinesterase inhibitors in Alzheimer’s disease, *Neuropharmacology* 190 (2021), 108352, <https://doi.org/10.1016/j.neuropharm.2020.108352>.
- [8] M. Tolar, S. Abushakra, J.A. Hey, A. Porsteinsson, M. Sabbagh, Aducanumab, gantenerumab, BAN2401, and ALZ-801 - the first wave of amyloid-targeting drugs for Alzheimer’s disease with potential for near term approval, *Alzheimer’s Res. Ther.* 12 (2020) 1–10, <https://doi.org/10.1186/s13195-020-00663-w>.
- [9] I.P.C. Gunawardena, T. Retinasamy, MohdF. Shaikh, Is aducanumab for LMICs? Promises and challenges, *Brain Sci.* 11 (2021) 1547, <https://doi.org/10.3390/brainsci11111547>.
- [10] E.S. Mitchell, J.F. Neumaier, 5-HT6 receptors: a novel target for cognitive enhancement, *Pharmacol. Ther.* 108 (2005) 320–333, <https://doi.org/10.1016/j.pharmthera.2005.05.001>.
- [11] W.J. Geldenhuys, C.J. Van Der Schyf, Role of serotonin in alzheimer’s disease A new therapeutic target, *CNS Drugs* 25 (2011) 765–781.
- [12] G. Koch, Modulating 5-HT4 and 5-HT6 receptors in Alzheimer’s disease treatment, *Future Med. Chem.* 71 (2017) 643, <https://doi.org/10.2307/j.ctvncw0d0.18>.
- [13] K. Kucwaj-Brysz, H. Baltrukewich, K. Czarnota, J. Handzlik, Chemical update on the potential for serotonin 5-HT6 and 5-HT7 receptor agents in the treatment of Alzheimer’s disease, *Bioorg. Med. Chem. Lett* 49 (2021), 128275, <https://doi.org/10.1016/j.bmcl.2021.128275>.
- [14] A.M. Bokare, M. Bhonde, R. Goel, Y. Nayak, 5-HT6 receptor agonist and antagonist modulates ICV-STZ-induced memory impairment in rats, *Psychopharmacology (Berl)* 235 (2018) 1557–1570, <https://doi.org/10.1007/s00213-018-4866-z>.
- [15] S. Sudoi, K. Kucwaj-Brysz, R. Kurczab, N. Wilczyńska, M. Jastrzębska-Więsek, G. Satała, G. Latacz, M. Gluch-Lutwin, B. Mordyl, E. Żesławska, W. Nitek, A. Partyka, K. Buzun, A. Doroz-Plonka, A. Wesołowska, A. Bielawska, J. Handzlik, Chlorine substituents and linker topology as factors of 5-HT6R activity for novel highly active 1,3,5-triazine derivatives with procognitive properties in vivo, *Eur. J. Med. Chem.* 203 (2020), <https://doi.org/10.1016/j.ejmech.2020.112529>.
- [16] H. Bulut, S. Hattori, H. Aoki-ogata, H. Hayashi, Single atom changes in newly synthesized HIV protease inhibitors reveal structural basis for extreme affinity, high genetic barrier, and adaptation to the HIV protease plasticity, *Sci. Rep.* 10 (2020) 1–12, <https://doi.org/10.1038/s41598-020-65993-z>.
- [17] H. Busto, S. Castillo, M. Escudero-casao, A. Avenoza, J.L. Asensio, G. Jime, O. Bouteira, R. Fiamengo, Structure-based design of potent tumor-associated antigens: modulation of peptide presentation by single-atom O/S or O/Se substitutions at the glycosidic linkage, *J. Am. Chem. Soc.* 141 (2019) 4063–4072, <https://doi.org/10.1021/jacs.8b13503>.
- [18] H. Nagaoka, H. Nishiwaki, T. Kubo, M. Akamatsu, S. Yamauchi, Docking model of the nicotinic acetylcholine receptor and nitromethylene neonicotinoid derivatives with a longer chiral substituent and their biological activities, *Bioorg. Med. Chem.* 23 (2015) 759–769, <https://doi.org/10.1016/j.bmc.2014.12.058>.
- [19] A. Kozlova, L. Thabault, N. Dauguet, M. Deskeuvre, Investigation of chalcogen bioisosteric replacement in a series of heterocyclic inhibitors of tryptophan 2, 3-dioxygenase, *Eur. J. Med. Chem.* 227 (2022) 1–12, <https://doi.org/10.1016/j.ejmech.2021.113892>.
- [20] L. Moroder, Isosteric replacement of sulfur with other chalcogens in peptides and proteins, *J. Pept. Sci.* 214 (2005) 187–214, <https://doi.org/10.1002/psc.654>.
- [21] M.R. Koebel, A. Cooper, G. Schmadeke, S. Jeon, M. Narayan, S. Sirimulla, S. O and S ... N sulfur bonding interactions in protein – ligand complexes: empirical considerations and scoring function, *J. Chem. Inf. Model.* 56 (2016) 2298–2309, <https://doi.org/10.1021/acs.jcim.6b00236>.
- [22] N. Brown, *Part One Principles Bioisosterism in Medicinal Chemistry*, 2012.
- [23] S. Sudoi, A. Cios, M. Jastrz, The phenoxyalkyltriazine antagonists for 5-HT 6 receptor with promising procognitive and pharmacokinetic properties in vivo in search for a novel therapeutic approach to dementia diseases, *Int. J. Mol. Sci.* 22 (2021), 10773.
- [24] W. Ali, M. Więcek, D. Łażewska, R. Kurczab, M. Jastrzębska-Więsek, G. Satała, K. Kucwaj-Brysz, A. Lubelska, M. Gluch-Lutwin, B. Mordyl, A. Siwek, M.J. Nasim, A. Partyka, S. Sudoi, G. Latacz, A. Wesołowska, K. Kieć-Kononowicz, J. Handzlik, Synthesis and computer-aided SAR studies for derivatives of phenoxyalkyl-1,3,5-triazine as the new potent ligands for serotonin receptors 5-HT6, *Eur. J. Med. Chem.* 178 (2019) 740–751, <https://doi.org/10.1016/j.ejmech.2019.06.022>.
- [25] D. Łażewska, R. Kurczab, M. Więcek, G. Satała, K. Kieć-Kononowicz, J. Handzlik, Synthesis and computer-aided analysis of the role of linker for novel ligands of the 5-HT 6 serotonin receptor among substituted 1,3,5-triazinylpiperazines, *Bioorg. Chem.* 84 (2019) 319–325, <https://doi.org/10.1016/j.bioorg.2018.11.046>.
- [26] S. Thavaneswaran, K. Mccamley, P.J. Scammells, N-demethylation of alkaloids, *Nat. Prod. Commun.* 1 (2006) 885–897.
- [27] B.P. Guiard, G. Di Giovanni, Central serotonin-2A (5-HT2A) receptor dysfunction in depression and epilepsy: the missing link? *Front. Pharmacol.* 6 (2015) <https://doi.org/10.3389/fphar.2015.00046>.
- [28] A. Zięba, P. Stepnicki, D. Matosiuk, A.A. Kaczor, Overcoming depression with 5-HT2a receptor ligands, *Int. J. Mol. Sci.* 23 (2022), <https://doi.org/10.3390/ijms23010010>.
- [29] I. Espadas, O. Ortiz, P. Garcia-Sanz, A. Sanz-Magro, S. Alberquilla, O. Solis, J. M. Delgado-Garcia, A. Gruart, R. Moratalla, Dopamine D2R is required for

- hippocampal-dependent memory and plasticity at the CA3-CA1 synapse, *Cerebr. Cortex* 31 (2021) 2187–2204, <https://doi.org/10.1093/cercor/bhaa354>.
- [30] G. Zhang, R.W. Stackman, The role of serotonin 5-HT_{2A} receptors in memory and cognition, *Front. Pharmacol.* 6 (2015), <https://doi.org/10.3389/fphar.2015.00225>.
- [31] R. Pakdel, A. Rashidy-Pour, Glucocorticoid-induced impairment of long-term memory retrieval in rats: an interaction with dopamine D2 receptors, *Neurobiol. Learn. Mem.* 85 (2006) 300–306, <https://doi.org/10.1016/j.nlm.2005.12.003>.
- [32] D. Łazewska, R. Kurczab, M. Więcek, K. Kamińska, G. Satała, M. Jastrzębska-Więsek, A. Partyka, A.J. Bojarski, A. Wesolowska, K. Kieć-Kononowicz, J. Handzlik, The computer-aided discovery of novel family of the 5-HT₆ serotonin receptor ligands among derivatives of 4-benzyl-1,3,5-triazine, *Eur. J. Med. Chem.* 135 (2017) 117–124, <https://doi.org/10.1016/j.ejmech.2017.04.033>.
- [33] A. Lubelska, G. Latacz, M. Jastrzębska-Więsek, M. Kotańska, R. Kurczab, A. Partyka, M.A. Mańc, D. Wilczyńska, A. Doroz-Plonka, D. Łazewska, A. Wesolowska, K. Kieć-Kononowicz, J. Handzlik, Are the hydantoin-1,3,5-triazine 5-HT_{6R} ligands a hope to a find new procognitive and anti-obesity drug? Considerations based on primary in vivo assays and ADME-tox profile in vitro, *Molecules* 24 (2019), <https://doi.org/10.3390/molecules24244472>.
- [34] A. Kumar, A. Singh, Ekavali, A review on Alzheimer's disease pathophysiology and its management: an update, *Pharmacol. Rep.* 67 (2015) 195–203, <https://doi.org/10.1016/j.pharep.2014.09.004>.
- [35] R. Purgatorio, M. de Candia, M. Catto, A. Carrieri, L. Pisani, A. De Palma, M. Toma, O.A. Ivanova, L.G. Voskressensky, C.D. Altomare, Investigating 1,2,3,4,5,6-hexahydroazepino[4,3-b]indole as scaffold of butyrylcholinesterase-selective inhibitors with additional neuroprotective activities for Alzheimer's disease, *Eur. J. Med. Chem.* 177 (2019) 414–424, <https://doi.org/10.1016/j.ejmech.2019.05.062>.
- [36] M. de Candia, G. Zaetta, N. Denora, D. Tricarico, M. Majellaro, S. Cellamare, C. D. Altomare, New azepino[4,3-b]indole derivatives as nanomolar selective inhibitors of human butyrylcholinesterase showing protective effects against NMDA-induced neurotoxicity, *Eur. J. Med. Chem.* 125 (2017) 288–298, <https://doi.org/10.1016/j.ejmech.2016.09.037>.
- [37] Y. Nicolet, O. Lockridge, P. Masson, J.C. Fontecilla-Camps, F. Nachon, Crystal structure of human butyrylcholinesterase and of its complexes with substrate and products, *J. Biol. Chem.* 278 (2003) 41141–41147, <https://doi.org/10.1074/jbc.M210241200>.
- [38] S.Y. Chioi, T.T. Weng, G.Z. Lin, R.J. Lu, S.Y. Jian, G. Lin, Molecular docking of different inhibitors and activators to butyrylcholinesterase, *J. Biomol. Struct. Dyn.* 33 (2015) 563–572, <https://doi.org/10.1080/07391102.2014.896749>.
- [39] R. Purgatorio, M. de Candia, M. Catto, M. Rullo, L. Pisani, N. Denora, A. Carrieri, A.A. Nevskaya, L.G. Voskressensky, C.D. Altomare, Evaluation of water-soluble mannich base prodrugs of 2,3,4,5-Tetrahydroazepino[4,3-b]indol-1(6H)-one as multitarget-directed agents for alzheimer's disease, *ChemMedChem* 16 (2021) 589–598, <https://doi.org/10.1002/cmdc.202000583>.
- [40] R. Purgatorio, N. Gambacorta, M. de Candia, M. Catto, M. Rullo, L. Pisani, O. Nicolotti, C.D. Altomare, First-in-class isonipicotamide-based thrombin and cholinesterase dual inhibitors with potential for Alzheimer disease, *Molecules* 26 (2021), <https://doi.org/10.3390/molecules26175208>.
- [41] M. Rossi, M. Freschi, L. De Camargo Nascente, A. Salerno, S. De Melo Viana Teixeira, F. Nachon, F. Chantegreil, O. Soukup, L. Prchal, M. Malaguti, C. Bergamini, M. Bartolini, C. Angeloni, S. Hrelia, L.A. Soares Romeiro, M. L. Bolognesi, Sustainable drug discovery of multi-target-directed ligands for alzheimer's disease, *J. Med. Chem.* 64 (2021) 4972–4990, <https://doi.org/10.1021/acs.jmedchem.1c00048>.
- [42] J. Sniwickowska, M. Gluch-lutwin, A. Bucki, A. Wi, A. Siwek, K. Pytka, G. Latacz, M. Jastrzębska-więsek, A. Partyka, D. Wilczyn, A. Weso, M. Paw, K. Przejczowska-pomierny, Discovery of novel pERK1/2- or β -arrestin-preferring 5-HT₂, *J. Med. Chem.* 63 (2020) 10946–11071, <https://doi.org/10.1021/acs.jmedchem.0c00814>.
- [43] H. Sun, E.C.Y. Chow, S. Liu, Y. Du, K.S. Pang, The Caco-2 cell monolayer: usefulness and limitations, *Expet Opin. Drug Metabol. Toxicol.* 4 (2008) 395–411, <https://doi.org/10.1517/17425255.4.4.395>.
- [44] D.A. Volpe, P.J. Faustino, A.B. Giavarella, E.B. Asafu-Adjaye, C.D. Ellison, L.X. Yu, A.S. Hussain, Classification of drug permeability with a Caco-2 cell monolayer assay, *Clin. Res. Regul. Aff.* 24 (2007) 39–47, <https://doi.org/10.1080/10601330701273669>.
- [45] A. Carocci, M. Roselli, R. Budriesi, M. Micucci, J.F. Desaphy, C. Altamura, M. M. Cavalluzzi, M. Toma, G.I. Passeri, G. Milani, A. Lovece, A. Catalano, C. Bruno, A. De Palma, F. Corbo, C. Franchini, S. Habtemariam, G. Lentini, Synthesis and evaluation of voltage-gated sodium channel blocking pyrrolidine derivatives endowed with both antiarrhythmic and antioxidant activities, *ChemMedChem* 16 (2021) 578–588, <https://doi.org/10.1002/cmdc.202000692>.
- [46] A.E. Enciso, B. Neun, J. Rodriguez, A.P. Ranjan, M.A. Dobrowolska, E. E. Simanek, Nanoparticle effects on human platelets in vitro: a comparison between PAMAM and triazine dendrimers, *Molecules* 21 (2016), <https://doi.org/10.3390/molecules21040428>.
- [47] M. Marcinkowska, M. Kubacka, A. Zagorska, A. Jaromin, N. Fajkis-Zajczkowska, M. Kolaczowski, Exploring the antiplatelet activity of serotonin 5-HT_{2A} receptor antagonists bearing 6-fluorobenzo [d] isoxazol-3-yl) propyl) motif – as potential therapeutic agents in the prevention of cardiovascular diseases, *Biomed. Pharmacother.* 145 (2022), 112424, <https://doi.org/10.1016/j.biopha.2021.112424>.
- [48] K.C.F. Fone, An update on the role of the 5-hydroxytryptamine₆ receptor in cognitive function, *Neuropharmacology* 55 (2008) 1015–1022, <https://doi.org/10.1016/j.neuropharm.2008.06.061>.
- [49] J. Rychtyk, A. Partyka, J. Gdula-Argasińska, K. Mystowska, N. Wilczyńska, M. Jastrzębska-Więsek, A. Wesolowska, 5-HT₆ receptor agonist and antagonist improve memory impairments and hippocampal BDNF signaling alterations induced by MK-801, *Brain Res.* 1722 (2019), <https://doi.org/10.1016/j.brainres.2019.146375>.
- [50] F.J. van der Staay, K. Rutten, C. Erb, A. Blokland, Effects of the cognition impairer MK-801 on learning and memory in mice and rats, *Behav. Brain Res.* 220 (2011) 215–229, <https://doi.org/10.1016/j.bbr.2011.01.052>.
- [51] A. Adell, L. Jiménez-Sánchez, X. López-Gil, T. Romón, Is the acute NMDA receptor hypofunction a valid model of schizophrenia? *Schizophr. Bull.* 38 (2012) 9–14, <https://doi.org/10.1093/schbul/sbr133>.
- [52] D. Karila, T. Freret, V. Bouet, M. Boulouard, P. Dallemagne, C. Rochais, Therapeutic potential of 5-HT₆ receptor agonists, *J. Med. Chem.* 58 (2015) 7901–7912, <https://doi.org/10.1021/acs.jmedchem.5b00179>.
- [53] M.V. King, C.A. Marsden, K.C.F. Fone, A role for the 5-HT_{1A}, 5-HT₄ and 5-HT₆ receptors in learning and memory, *Trends Pharmacol. Sci.* 29 (2008) 482–492, <https://doi.org/10.1016/j.tips.2008.07.001>.
- [54] M.V. King, A.J. Sleight, M.L. Woolley, I.A. Topham, C.A. Marsden, K.C.F. Fone, 5-HT₆ receptor antagonists reverse delay-dependent deficits in novel object discrimination by enhancing consolidation – an effect sensitive to NMDA receptor antagonism, *Neuropharmacology* 47 (2004) 195–204, <https://doi.org/10.1016/j.neuropharm.2004.03.012>.
- [55] W.D. Hirst, T.O. Stean, D.C. Rogers, D. Sunter, P. Pugh, S.F. Moss, S.M. Bromidge, G. Riley, D.R. Smith, S. Bartlett, C.A. Heidbreder, A.R. Atkins, L.P. Lacroix, L. A. Dawson, A.G. Foley, C.M. Regan, N. Upton, SB-399885 is a potent, selective 5-HT₆ receptor antagonist with cognitive enhancing properties in aged rat water maze and novel object recognition models, *Eur. J. Pharmacol.* 553 (2006) 109–119, <https://doi.org/10.1016/j.ejphar.2006.09.049>.
- [56] S. Woods, N.N. Clarke, R. Layfield, K.C.F. Fone, 5-HT₆ receptor agonists and antagonists enhance learning and memory in a conditioned emotion response paradigm by modulation of cholinergic and glutamatergic mechanisms, *Br. J. Pharmacol.* 167 (2012) 436–449, <https://doi.org/10.1111/j.1476-5381.2012.02022.x>.
- [57] V. Da Silva Costa-Aze, A. Quiedeville, M. Boulouard, F. Dauphin, 5-HT₆ receptor blockade differentially affects scopolamine-induced deficits of working memory, recognition memory and aversive learning in mice, *Psychopharmacology (Berl)* 222 (2012) 99–115, <https://doi.org/10.1007/s00213-011-2627-3>.
- [58] N.M.W.J. de Bruin, J. Prickaerts, A. van Loevezijn, J. Venhorst, L. de Groot, P. Houba, O. Reneerkens, S. Akkerman, C.G. Kruse, Two novel 5-HT₆ receptor antagonists ameliorate scopolamine-induced memory deficits in the object recognition and object location tasks in Wistar rats, *Neurobiol. Learn. Mem.* 96 (2011) 392–402, <https://doi.org/10.1016/j.nlm.2011.06.015>.
- [59] J. Arnt, B. Bang-Andersen, B. Grayson, F.P. Bymaster, M.P. Cohen, N.W. Delapp, B. Giethlen, M. Kreilgaard, D.L. McKinzie, J.C. Neill, D.L. Nelson, S.M. Nielsen, M. N. Poulsen, J.M. Schaus, L.M. Witten, Lu AE58054, a 5-HT₆ antagonist, reverses cognitive impairment induced by subchronic phencyclidine in a novel object recognition test in rats, *Int. J. Neuropharmacol.* 13 (2010) 1021–1033, <https://doi.org/10.1017/S1461145710000659>.
- [60] K. Kucwaj-Brysz, W. Ali, R. Kurczab, S. Sudoł-Talaj, N. Wilczyńska-Zawal, M. Jastrzębska-Więsek, G. Satała, B. Mordyl, E. Żesławska, Agnieszka-Olejarz-Maciej, K. Czarnota, G. Latacz, A. Partyka, A. Wesolowska, W. Nitek, J. Handzlik, An exit beyond the pharmacophore model for 5-HT_{6R} agents – a new strategy to gain dual 5-HT₆/5-HT_{2A} action for triazine derivatives with procognitive potential, *Bioorg. Chem.* 121 (2022), <https://doi.org/10.1016/j.bioorg.2022.105695>.
- [61] S. Salim, Oxidative stress and the central nervous system, *J. Pharmacol. Exp. Therapeut.* 360 (2017) 201–205, <https://doi.org/10.1124/jpet.116.237503>.
- [62] D.M. Teleanu, A.G. Niculescu, I.I. Lungu, C.I. Radu, O. Vladăncescu, E. Roza, B. Costăchescu, A.M. Grumezescu, R.I. Teleanu, An overview of oxidative stress, neuroinflammation and neurodegenerative diseases, *Int. J. Mol. Sci.* 23 (2022), <https://doi.org/10.3390/ijms23115938>.
- [63] A. Singh, R. Kukreti, L. Saso, S. Kukreti, Oxidative stress: a key modulator in neurodegenerative diseases, *Molecules* 24 (2019), <https://doi.org/10.3390/molecules24081583>.
- [64] A. Merelli, M. Repetto, A. Lazarowski, J. Auzmendi, Hypoxia, oxidative stress, and inflammation: three faces of neurodegenerative diseases, *J. Alzheim. Dis.* 82 (2021), <https://doi.org/10.3233/JAD-201074>. S109–S126.
- [65] Z. Chen, C. Zhong, Oxidative stress in Alzheimer's disease, *Neurosci. Bull.* 30 (2014) 271–281, <https://doi.org/10.1007/s12264-013-1423-y>.
- [66] G.F. Ecker, C.R. Noe, *In Silico Prediction Models for Blood-Brain Barrier Permeation*, 2004.
- [67] Y.H. Zhao, M.H. Abraham, A. Ibrahim, P.V. Fish, S. Cole, M.L. Lewis, M.J. De Groot, D.P. Reynolds, Predicting penetration across the blood-brain barrier from simple descriptors and fragmentation schemes, *J. Chem. Inf. Model.* 47 (2007) 170–175, <https://doi.org/10.1021/ci600312d>.
- [68] F.M.G. Cornelissen, G. Markert, G. Deutsch, M. Antonara, N. Faaij, I. Bartelink, D. Noske, W.P. Vandertop, A. Bender, B.A. Westerman, Explaining blood-brain barrier permeability of small molecules by integrated analysis of different transport mechanisms, *J. Med. Chem.* 66 (2023) 7253–7267, <https://doi.org/10.1021/acs.jmedchem.2c01824>.
- [69] D.E.V. Pires, T.L. Blundell, D.B. Ascher, pkCSM: predicting small-molecule pharmacokinetic and toxicity properties using graph-based signatures, *J. Med. Chem.* 58 (2015) 4066–4072, <https://doi.org/10.1021/acs.jmedchem.5b00104>.
- [70] A. Daina, O. Michielin, V. Zoete, SwissADME: a free web tool to evaluate pharmacokinetics, drug likeness and medicinal chemistry friendliness of small molecules, *Sci. Rep.* 7 (2017), 42717, <https://doi.org/10.1038/srep42717>.

- [71] G.M. Sheldrick, Shelxt - integrated space-group and crystal-structure determination, *Acta Crystallogr. A* 71 (2015) 3–8, <https://doi.org/10.1107/S2053273314026370>.
- [72] M.C. Burla, R. Caliandro, B. Carrozzini, G.L. Cascarano, C. Cuocci, G. Giacovazzo, M. Mallamo, A. Mazzzone, G. Polidori, Crystal structure determination and refinement via SIR2014, *J. Appl. Crystallogr.* 48 (2015) 306–309, <https://doi.org/10.1107/S1600576715001132>.
- [73] G.M. Sheldrick, Crystal structure refinement with SHELXL, *Acta Crystallogr. C Struct. Chem* 71 (2015) 3–8, <https://doi.org/10.1107/S2053229614024218>.
- [74] Y.-C. Cheng, W.H. Prusoff, Relationship between the Inhibition Constant (K_i) and the Concentration of Inhibitor Which Causes 50 Per Cent Inhibition (I₅₀) of an Enzymatic Reaction, Pergamon Press, 1973.
- [75] S. Huang, P. Xu, D.D. Shen, I.A. Simon, C. Mao, Y. Tan, H. Zhang, K. Harpsøe, H. Li, Y. Zhang, C. You, X. Yu, Y. Jiang, Y. Zhang, D.E. Gloriam, H.E. Xu, GPCRs steer G_i and G_s selectivity via TM5-TM6 switches as revealed by structures of serotonin receptors, *Mol. Cell.* 82 (2022) 2681–2695.
- [76] S.K. Burley, C. Bhikadiya, C. Bi, S. Bittrich, H. Chao, L. Chen, P.A. Craig, G. V. Crichlow, K. Dalenberg, J.M. Duarte, S. Dutta, M. Fayazi, Z. Feng, J.W. Flatt, S. Ganesan, S. Ghosh, D.S. Goodsell, R.K. Green, V. Guranovic, J. Henry, B. P. Hudson, I. Khokhriakov, C.L. Lawson, Y. Liang, R. Lowe, E. Peisach, I. Persikova, D.W. Pielh, Y. Rose, A. Sali, J. Segura, M. Sekharan, C. Shao, B. Vallat, M. Voigt, B. Webb, J.D. Westbrook, S. Whetstone, J.Y. Young, A. Zalevsky, C. Zardecki, RCSB Protein Data Bank (RCSB.org): delivery of experimentally-determined PDB structures alongside one million computed structure models of proteins from artificial intelligence/machine learning, *Nucleic Acids Res.* 51 (2023) D488–D508, <https://doi.org/10.1093/nar/gkac1077>.
- [77] B. Kevin J, C. Edmond, X. Huafeng, D. Ron O, E. Michael P, G. Brent A, K. John L, K. Istvan, M. Mark A, S. Federico D, S. John K, S. Yibing, S. David E, Scalable algorithms for molecular dynamics simulations on commodity clusters, in: Proceedings of the ACM/IEEE SC 2006 Conference (SC'06), vol. 43, 2006, <https://doi.org/10.1145/1188455.1188544>. Tampa, FL, USA.
- [78] M.A. Lomize, I.D. Pogozheva, H. Joo, H.I. Mosberg, A.L. Lomize, OPM database and PPM web server: resources for positioning of proteins in membranes, *Nucleic Acids Res.* 40 (2012), <https://doi.org/10.1093/nar/gkr703>.
- [79] J. Contreras-García, E.R. Johnson, S. Keinan, R.P. Piquemal, D. N. Beratan, W. Yang, NCIPLLOT: a program for plotting noncovalent interaction regions, *J. Chem. Theor. Comput.* 7 (2011) 625–632, <https://doi.org/10.1021/ct100641a>.
- [80] M.J. et al Frisch, Gaussian 16, Revision D.01., ((n.d.)).
- [81] A.D. Becke, Density-functional thermochemistry. III. The role of exact exchange, *J. Chem. Phys.* 98 (1993) 5648–5652, <https://doi.org/10.1063/1.464913>.
- [82] P.J. Stephens, F.J. Devlin, C.F. Chabalowski, M.J. Frisch, Ab initio calculation of vibrational absorption and circular dichroism spectra using density functional force fields, *J. Phys. Chem.* 98 (1994) 11623–11627, <https://doi.org/10.1021/j100096a001>.
- [83] S. Grimme, J. Antony, S. Ehrlich, H. Krieg, A consistent and accurate ab initio parametrization of density functional dispersion correction (DFT-D) for the 94 elements H-Pu, *J. Chem. Phys.* 132 (2010), 154104, <https://doi.org/10.1063/1.3382344>.
- [84] T.H. Dunning, Gaussian basis sets for use in correlated molecular calculations. I. The atoms boron through neon and hydrogen, *J. Chem. Phys.* 90 (1989) 1007–1023, <https://doi.org/10.1063/1.456153>.
- [85] R.A. Kendall, T.H. Dunning, R.J. Harrison, Electron affinities of the first-row atoms revisited. Systematic basis sets and wave functions, *J. Chem. Phys.* 96 (1992) 6796–6806, <https://doi.org/10.1063/1.462569>.
- [86] S. Miertuš, E. Scrocco, J. Tomasi, Electrostatic interaction of a solute with a continuum. A direct utilization of AB initio molecular potentials for the prevision of solvent effects, *Chem. Phys.* 55 (1981) 117–129, [https://doi.org/10.1016/0301-0104\(81\)85090-2](https://doi.org/10.1016/0301-0104(81)85090-2).
- [87] B. Mennucci, R. Cammi, J. Tomasi, Analytical free energy second derivatives with respect to nuclear coordinates: complete formulation for electrostatic continuum solvation models, *J. Chem. Phys.* 110 (1999) 6858–6870, <https://doi.org/10.1063/1.478591>.
- [88] L.L.C. Schrödinger, Schrödinger Release 2023-1, Maestro, 2023.
- [89] QUACPAC 2.1.0.4, OpenEye Scientific Software, Santa Fe, NM, <http://www.eyesopen.com>, (n.d.).
- [90] N.M. O'Boyle, M. Banck, C.A. James, C. Morley, T. Vandermeersch, G. R. Hutchison, Open Babel: an open chemical toolbox. <http://www.jcheminf.com/content/3/1/33>, 2011.
- [91] O. Gerlits, K.Y. Ho, X. Cheng, D. Blumenthal, P. Taylor, A. Kovalevsky, Z. Radić, A new crystal form of human acetylcholinesterase for exploratory room-temperature crystallography studies, *Chem. Biol. Interact.* 309 (2019), <https://doi.org/10.1016/j.cbi.2019.06.011>.
- [92] S.K. Burley, H.M. Berman, C. Bhikadiya, C. Bi, L. Chen, L. Di Costanzo, C. Christie, J.M. Duarte, S. Dutta, Z. Feng, S. Ghosh, D.S. Goodsell, R.K. Green, V. Guranovic, D. Guzenko, B.P. Hudson, Y. Liang, R. Lowe, E. Peisach, I. Persikova, C. Randle, A. Rose, M. Sekharan, C. Shao, Y.P. Tao, Y. Valasatava, M. Voigt, J. Westbrook, J. Young, C. Zardecki, M. Zhuravleva, G. Kurisu, H. Nakamura, Y. Kengaku, H. Cho, J. Sato, J.Y. Kim, Y. Ikegawa, A. Nakagawa, R. Yamashita, T. Kudou, G. J. Bekker, H. Suzuki, T. Iwata, M. Yokochi, N. Kobayashi, T. Fujiwara, S. Velankar, G.J. Kleywegt, S. Anyango, D.R. Armstrong, J.M. Berrisford, M. J. Conroy, J.M. Dana, M. Deshpande, P. Gane, R. Gáborová, D. Gupta, A. Gutmanas, J. Koča, L. Mak, S. Mir, A. Mukhopadhyay, N. Nadzirin, S. Nair, A. Patwardhan, T. Paysan-Lafosse, L. Pravda, O. Salih, D. Sehnal, M. Varadi, R. Váreková, J.L. Markley, J.C. Hoch, P.R. Romero, K. Baskaran, D. Maziuk, E. L. Ulrich, J.R. Wedell, H. Yao, M. Livny, Y.E. Ioannidis, Protein Data Bank: the single global archive for 3D macromolecular structure data, *Nucleic Acids Res.* 47 (2019), <https://doi.org/10.1093/nar/gky949>. D520–D528.
- [93] W.D. Cornell, P. Cieplak, C.I. Bayly, I.R. Gould, K.M. Merz, D.M. Ferguson, D. C. Spellmeyer, T. Fox, J.W. Caldwell, P.A. Kollman, A second generation force field for the simulation of proteins, nucleic acids, and organic molecules, *J. Am. Chem. Soc.* 117 (1995) 5179–5197, <https://doi.org/10.1021/ja00124a002>.
- [94] G.M. Morris, D.S. Goodsell, R.S. Halliday, R. Huey, W.E. Hart, R.K. Belew, A. J. Olson, Automated docking using a Lamarckian genetic algorithm and an empirical binding free energy function, *J. Comput. Chem.* 19 (1998) 1639–1662.
- [95] L. El Khoury, D. Santos-Martins, S. Sasmal, J. Eberhardt, G. Bianco, F. A. Ambrosio, L. Solis-Vasquez, A. Koch, S. Forli, D.L. Mobley, Comparison of affinity ranking using AutoDock-GPU and MM-GBSA scores for BACE-1 inhibitors in the D3R Grand Challenge 4, *J. Comput. Aided Mol. Des.* 33 (2019) 1011–1020, <https://doi.org/10.1007/s10822-019-00240-w>.
- [96] S. Forli, A.J. Olson, A force field with discrete displaceable waters and desolvation entropy for hydrated ligand docking, *J. Med. Chem.* 55 (2012) 623–638, <https://doi.org/10.1021/jm2005145>.
- [97] A. Carocci, A. Barbarossa, R. Leuci, A. Carrieri, L. Brunetti, A. Laghezza, M. Catto, F. Limongelli, S. Chaves, P. Tortorella, C.D. Altomare, M.A. Santos, F. Loiodice, L. Piemontese, Novel phenothiazine/donepezil-like hybrids endowed with antioxidant activity for a multi-target approach to the therapy of Alzheimer's disease, *Antioxidants* 11 (2022), <https://doi.org/10.3390/antiox11091631>.
- [98] OpenEye Scientific Software, ROCS, 3.4.0.4, OpenEye Scientific Software, Santa Fe, NM, <http://www.eyesopen.com>, (n.d.).
- [99] G. Latacz, A. Lubelska, M. Jastrzębska-Więsek, A. Partyka, A. Sobito, A. Olejarz, K. Kucwaj-Brysz, G. Satała, A.J. Bojarski, A. Wesolowska, K. Kieć-Kononowicz, J. Handzlik, In the search for a lead structure among series of potent and selective hydantoin 5-HT₇R agents: the drug-likeness in vitro study, *Chem. Biol. Drug Des.* 90 (2017) 1295–1306, <https://doi.org/10.1111/cbdd.13106>.
- [100] D.A. Sykes, H. Moore, L. Stott, N. Holliday, J.A. Javitch, J. Robert Lane, S. J. Charlton, Extrapyramidal side effects of antipsychotics are linked to their association kinetics at dopamine D₂ receptors, *Nat. Commun.* 8 (2017), <https://doi.org/10.1038/s41467-017-00716-z>.
- [101] N. Zarefopoulos, C. Papatheodoropoulos, Effects of 5-HT₇ receptor ligands on memory and cognition, *Neurobiol. Learn. Mem.* 136 (2016) 204–209, <https://doi.org/10.1016/j.nlm.2016.10.011>.
- [102] G. Latacz, A. Lubelska, M. Jastrzębska-Więsek, A. Partyka, K. Kucwaj-Brysz, A. Wesolowska, K. Kieć-Kononowicz, J. Handzlik, MF-8, a novel promising arylpiperazine-hydantoin based 5-HT₇ receptor antagonist: in vitro drug-likeness studies and in vivo pharmacological evaluation, *Bioorg. Med. Chem. Lett* 28 (2018) 878–883, <https://doi.org/10.1016/j.bmcl.2018.02.003>.
- [103] I. Hubatsch, E.G.E. Ragnarsson, P. Artursson, Determination of drug permeability and prediction of drug absorption in Caco-2 monolayers, *Nat. Protoc.* 2 (2007) 2111–2119, <https://doi.org/10.1038/nprot.2007.303>.
- [104] D.A. Volpe, P.J. Faustino, A.B. Gavarella, E.B. Asafu-Adjaye, C.D. Ellison, L.X. Yu, A.S. Hussain, Classification of drug permeability with a Caco-2 cell monolayer assay, *Clin. Res. Regul. Aff.* 24 (2007) 39–47, <https://doi.org/10.1080/10601330701273669>.
- [105] G. Latacz, A.S. Hogendorf, A. Hogendorf, A. Lubelska, J.M. Wierońska, M. Woźniak, P. Cieślak, K. Kieć-Kononowicz, J. Handzlik, A.J. Bojarski, Search for a 5-CT alternative. In vitro and in vivo evaluation of novel pharmacological tools: 3-(1-alkyl-1H-imidazole-5-yl)-1H-indole-5-carboxamides, low-basicity 5-HT₇ receptor agonists, *Medchemcomm* 9 (2018) 1882–1890, <https://doi.org/10.1039/c8md00313k>.
- [106] K. Socała, S. Mogiński, M. Pieróg, D. Nieoczym, M. Abram, B. Szulczyk, A. Lubelska, G. Latacz, U. Doboszevska, P. Właż, K. Kamiński, KA-11, a novel pyrrolidine-2,5-dione derived broad-spectrum anticonvulsant: its antiepileptogenic, antinociceptive properties and in vitro characterization, *ACS Chem. Neurosci.* 10 (2019) 636–648, <https://doi.org/10.1021/acschemneuro.8b00476>.
- [107] H. Wang, J.A. Joseph, Original Contribution Quantifying Cellular Oxidative Stress by Dichlorofluorescein Assay Using Microplate Reader, 1999.
- [108] A. Ennaceur, J. Delacour, A new one-trial test for neurobiological studies of memory in rats. 1: behavioral data, *Behav. Brain Res.* 31 (1988) 47–59, [https://doi.org/10.1016/S0166-4328\(05\)80315-8](https://doi.org/10.1016/S0166-4328(05)80315-8).
- [109] P. Zajdel, T. Kos, K. Marciniec, G. Satała, V. Canale, K. Kamiński, M. Hołuj, T. Lenda, R. Koralewski, M. Bednarski, L. Nowiński, J. Wójcikowski, W.A. Daniel, A. Nikiforuk, I. Nalepa, P. Chmielarz, J. Kuśmierczyk, A.J. Bojarski, P. Popik, Novel multi-target azinesulfonamides of cyclic amine derivatives as potential antipsychotics with pro-social and pro-cognitive effects, *Eur. J. Med. Chem.* 145 (2018) 790–804, <https://doi.org/10.1016/j.ejmech.2018.01.002>.
- [110] R.D. Porsolt, A. Bertin, M. Jalfre, "Behavioural despair" in rats and mice: strain differences and the effects of imipramine, *Eur. J. Pharmacol.* 51 (1978) 291–294, <http://www.ncbi.nlm.nih.gov/pubmed/568552>. (Accessed 20 March 2015).
- [111] S. Pellow, S.E. File, Anxiolytic and anxiogenic drug effects on exploratory activity in an elevated plus-maze: a novel test of anxiety in the rat, *Pharmacol. Biochem. Behav.* 24 (1986) 525–529, <http://www.ncbi.nlm.nih.gov/pubmed/2871560>. (Accessed 13 March 2018).